REVIVING ABANDONED RESERVOIRS WITH HIGH-PRESSURE AIR INJECTION: APPLICATION IN A FRACTURED AND KARSTED DOLOMITE RESERVOIR

Semi-Annual Report

Reporting Period Start Date: October 1, 2002

Reporting Period End Date: March 31, 2003

Principal Authors: Robert Loucks (Co-PI), Steve Ruppel (Co-PI), Julia Gale, Jon Holder, Jon Olsen, Deanna Combs, Dhiraj Dembla, and Leonel Gomez

Date Report Issued: June 30, 2003

DOE Award Number: DE-FC26-02NT15442

Bureau of Economic Geology
Scott W. Tinker, Director
John A. and Katherine G. Jackson School of Geosciences
The University of Texas at Austin
Box X, University Station
Austin, TX 78713-8924

and

Goldrus Producing Company
17314 State Highway 249, Suite 300
Houston, Texas 77064-1140

June 2003

DISCLAIMER

ABSTRACT

The Bureau of Economic Geology and Goldrus Producing Company have assembled a multidisciplinary team of geoscientists and engineers to evaluate the applicability of high-pressure air injection (HPAI) in revitalizing a nearly abandoned carbonate reservoir in the Permian Basin of West Texas. The characterization phase of the project is utilizing geoscientists and petroleum engineers from the Bureau of Economic Geology and the Department of Petroleum Engineering (both at The University of Texas at Austin) to define the controls on fluid flow in the reservoir as a basis for developing a reservoir model. This model will be used to define a field deployment plan that Goldrus, a small independent oil company, will implement by drilling both vertical and horizontal wells during the demonstration phase of the project. Additional reservoir data are being gathered during the demonstration phase to improve the accuracy of the reservoir model. The results of the demonstration are being closely monitored to provide a basis for improving the design of the HPAI field deployment plan. The results of the reservoir characterization field demonstration and monitoring program will be documented and widely disseminated to facilitate adoption of this technology by oil operators in the Permian Basin and elsewhere in the U.S.

TABLE OF CONTENTS

FIGURES

I. INTRODUCTION

Despite declining production rates, existing reservoirs in the United States contain huge volumes of remaining oil that is not being effectively recovered. This oil resource constitutes a huge target for the development and application of modern, cost-effective technologies for producing oil. Chief among the barriers to the recovery of this oil are the high costs of designing and implementing conventional advanced recovery technologies in these mature, in many cases pressure-depleted, reservoirs. An additional, increasingly significant barrier is the lack of vital technical expertise that is necessary for the application of these technologies. This lack of expertise is especially notable among the small operators and independents that operate many of these mature, yet oil-rich reservoirs. We are addressing these barriers to more effective oil recovery by developing, testing, applying, and documenting an innovative technology that, when proven, can be used by even the smallest operator to significantly increase the flow of oil from mature U.S. reservoirs.

The Bureau of Economic Geology and Goldrus Producing Company have assembled a multidisciplinary team of geoscientists and engineers to evaluate the applicability of high-pressure air injection (HPAI) in revitalizing a nearly abandoned carbonate reservoir in the Permian Basin of West Texas. The Permian Basin, the largest oil-bearing basin in North America, contains more than 70 billion barrels of remaining oil in place and is an ideal venue to validate this technology. We have already demonstrated the potential of HPAI for oil recovery improved in preliminary laboratory tests and a reservoir pilot project. To more completely test the technology, this project is combining a detailed characterization of reservoir properties with a field demonstration and monitoring program to fully access the effectiveness and economics of HPAI.

The characterization phase of the project is utilizing geoscientists and petroleum engineers from the Bureau of Economic Geology and the Department of Petroleum Engineering (both at The University of Texas at Austin) to define the controls on fluid flow in the reservoir as a basis for developing a reservoir model. This model will be used to define a field deployment plan that Goldrus, a small independent oil company, will implement by drilling both vertical and horizontal wells during the demonstration phase of the project. Additional reservoir data are being gathered during

the demonstration phase to improve the accuracy of the reservoir model. The results of the demonstration will be closely monitored to provide a basis for improving the design of the HPAI field deployment plan. The results of the reservoir characterization field demonstration and monitoring program will be documented and widely disseminated to facilitate adoption of this technology by oil operators in the Permian Basin and elsewhere in the U.S.

The successful development of high-pressure air injection technology has tremendous potential for increasing the flow of oil from deep carbonate reservoirs in the Permian Basin, a target resource that can be conservatively estimated at more than 1.5 billion barrels. Successful implementation in the field chosen for demonstration, for example, could result in the recovery of more than 34 million barrels of oil that will not otherwise be recovered.

II. EXECUTIVE SUMMARY

The Bureau of Economic Geology and Goldrus Producing Company have assembled a multidisciplinary team of geoscientists and engineers to evaluate the applicability of high-pressure air injection (HPAI) in revitalizing a nearly abandoned carbonate reservoir in the Permian Basin of West Texas. The characterization phase of the project is utilizing geoscientists and petroleum engineers from the Bureau of Economic Geology and the Department of Petroleum Engineering (both at The University of Texas at Austin) to define the controls on fluid flow in the reservoir as a basis for developing a reservoir model. This model will be used to define a field deployment plan that Goldrus, a small independent oil company, will implement by drilling both vertical and horizontal wells during the demonstration phase of the project.

Barnhart Ellenburger field is located in the southeast corner of Reagan County, Texas. The Ellenburger at Barnhart field has undergone a complex history of fracturing and karsting associated with a composite unconformity and several periods of burial and uplift. Accordingly, high-resolution stratigraphic correlations are difficult. However, we successfully used SP and resistivity log signatures from 105 wells in the field to correlate multiple zones of moderate porosity

that appear to be laterally continuous throughout parts of the field. Regions in which log-signature correlations break down are interpreted to correspond to zones of brecciation and fracturing caused by karsting, strata dissolution (cave formation), and collapse. Recognition that apparent breaks in correlations may define karst and collapse breccias provides a potential basis for the mapping of subsurface karst features.

The following paleocave facies have been described: (1) collapsed ceiling facies; facies; (2) cave-fill, coarse-clast chaotic breccia facies; (3) cave-fill, fine-clast chaotic breccia facies; and (4) cave-sediment fill facies. The host rock and disturbed host rock facies were not cored in this well, but wireline logs and core photographs from another part of the field indicate that these facies may make up much of the field. The pore types noted in the Goldrus Producing Company Unit #3 core consists of (1) original matrix pores in clasts, (2) interclast pores, (3) crackle-breccia pores, (4) mosaic-breccia pores, (5) cave-sediment fill interparticle pores, (6) solution-vug pores, and (7) tectonic fracture pores. The mean porosity within the coalesced collapsed paleocave facies is 4.8% and ranges from 1.2% to 19.7%. The mean permeability is 3.4 md and ranges from 0.02 to 48.2 md. These values are typical of Ellenburger dolomite reservoirs in West Texas. The collapsed paleocave facies described in the Goldrus Producing Company Unit #3 core have been calibrated to the wireline and image logs. This calibration has produced a collapsed-paleocave type-log section that allows the recognition of nonhost rock sections. Combining this type-log section with other correlation techniques is aiding in defining the distribution of karsted sections in Barnhart field.

Fractures that crosscut clasts and cement and, therefore, postdate brecciation were identified in the Unit #3 core. These fractures form continuous features in the core and have been identified on image logs in this well. Results from sidewall cores and borehole images from a recent well confirmed the orientation of two sets of fractures (S70E/90 and S30W/90) in Barnhart field. These fracture sets appear to be broadly synchronous, but their origin has not yet been determined. They may be related to late-stage cave that collapse or to some more regionally widespread tectonic event.

Laboratory testing is being carried out to quantitatively assess mechanical alterations of reservoir material by the elevated temperatures near the combustion front. Samples of core material were heated in steps of 100°C up to nominal in situ combustion temperatures of 600°C without confining pressure. Compressional wave velocity in rock is sensitive to crack density, and wave velocities in the test specimens were measured at room temperature following each temperature excursion. Observations suggest that thermal alteration would be strongly influenced by the existence of prior fracture events. This conclusion is based on preliminary experimentation but has some basis in theory: thermally generated microfractures are primarily related to local heterogeneities in thermal expansion, and infill of naturally fractured rock should result in a greater degree of heterogeneity.

The two prototype heating tests described earlier were carried out on material in a completely unconfined state. It is known that fracturing is suppressed by confining stress, and a core holder has been fabricated to provide for heating under confined conditions. None of the specimens so far tested under confined conditions showed any evidence of thermally induced microfracturing (i.e., no reduction in wave velocity), although all of the Ellenburger specimens indicated significant thermal damage. More testing needs to be completed before reliable conclusions can be made and integrated into a reservoir model.

The project is on schedule (Fig. 1), and significant results will be obtained by the end of the year. The additional core and well data that Goldrus Producing Company will obtain this summer will greatly enhance our rock database.

III. OBJECTIVES

The primary objectives of the project are to develop, test, and document optimal methods for deploying high-pressure air injection (HPAI) technology to recover remaining hydrocarbons from an abandoned carbonate reservoir. Each of these will be accomplished in three phases of activity. The reservoir characterization phase (Phase 1) will consist of (1) analysis of reservoir stratigraphy and facies, (2) characterization and modeling of reservoir matrix petrophysical properties,

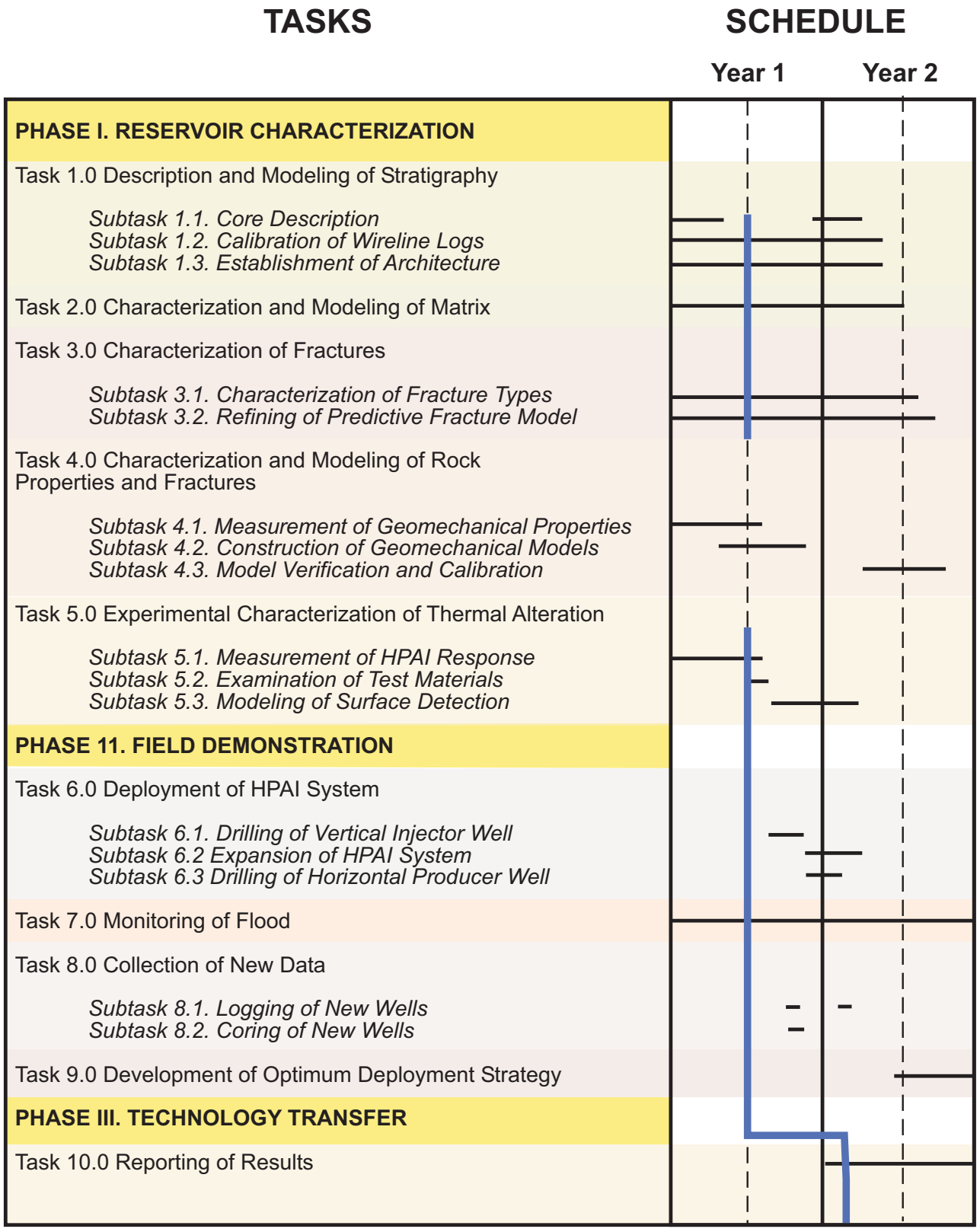

Figure 1. Project task schedule. Blue line is where the project is relative to the schedule.

(3) characterization and modeling of reservoir fractures, and (4) characterization and modeling of the effects of HPAI on reservoir mechanical properties (deformation, strength, and fluid transport behavior) for both matrix and fractures. The demonstration phase (Phase 2) will include (1) deployment of vertical HPAI injector wells and horizontal oil-producing wells on the basis of stratigraphic, petrophysical, fracture, and rock mechanical models developed in Phase 1; (2) collection of additional reservoir data to further constrain and revise existing models; (3) field monitoring of the progress of HPAI using well tests; and (4) postmortem analysis and synthesis of the best strategies for deployment of HPAI well patterns. The third and final phase of the project (Phase 3, Technology Transfer) will be devoted to compiling, reporting, and distributing the results of the completed project to industry.

IV. PHASE 1: RESERVOIR CHARACTERIZATION

Objectives of the reservoir characterization phase of the project are to provide the basic data for defining the distribution of key reservoir properties that control the distribution of remaining oil and the movement of injected air. Among the key issues that must be addressed in this phase are: (1) distribution of karst features and their impact on flow; (2) distribution, abundance, and orientation of fractures and their impact on flow; and (3) rock mechanics response of the Ellenburger to HPAI.

IV-1. General Geology

Barnhart Ellenburger field, located in the southeast corner of Reagan County, Texas (Fig. 2), was discovered in 1941 and produces from the Lower Ordovician Ellenburger Group. Most of the reservoir is dolomite, although some limestone sections exist. The field is approximately 93 sq. km (36 sq. mi) in size, has four-way structural closure (> 100 m; > 300 ft) (Fig. 3), and is sealed by the Wolfcampian shale. A composite unconformity forms the contact between the Lower Ordovician Ellenburger and the overlying Permian Wolfcampian shale. The average porosity and permeability within the field are 3.2 % and 7 millidarcys (md), respectively.

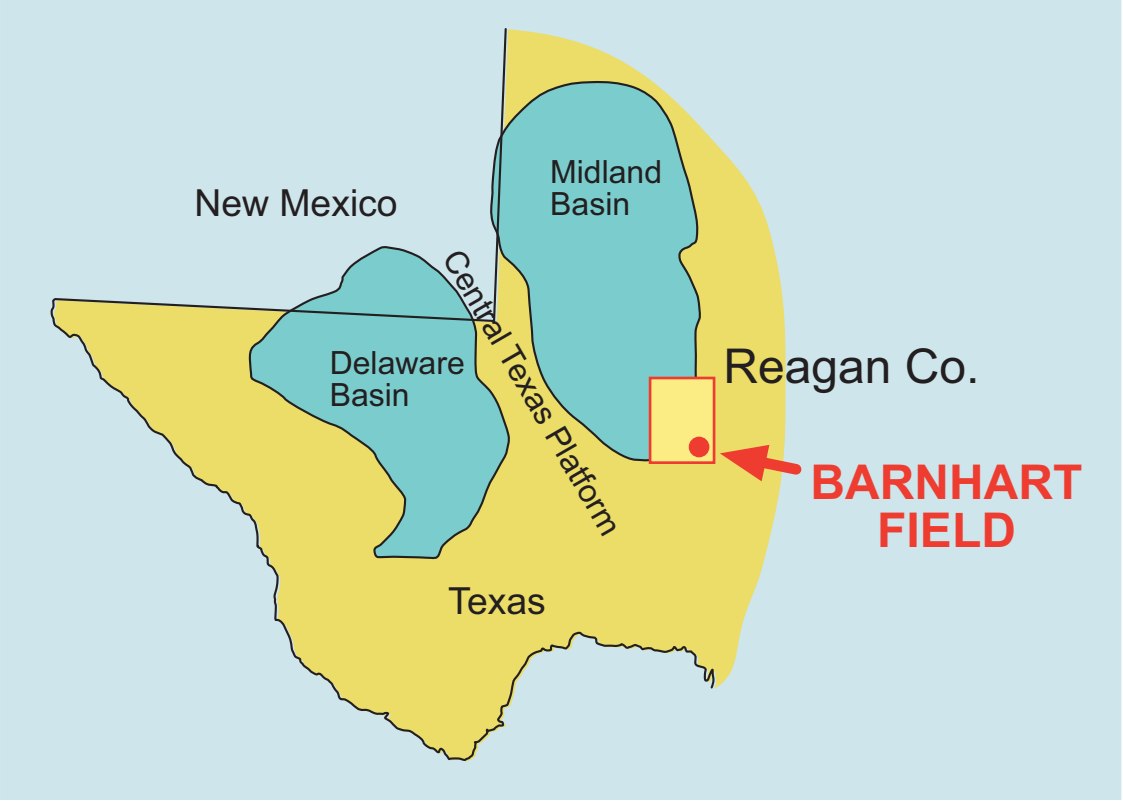

Figure 2. Regional map of Permian Basin showing the location of Barnhart field. The Delaware Basin, Central Basin Platform, and Midland Basin are included only for orientation purposes and are not intended to imply that they existed when Ellenburger strata were deposited.

The Ellenburger at Barnhart field has undergone a complex history of fracturing and karsting associated with a composite unconformity and several periods of burial and uplift (Fig. 4). This history is evident from the description of the Goldrus Unit #3 well core (discussed later), but the extent of these karst-related breccias in the field is not obvious. Because Barnhart field was developed primarily in the 1940's and 1950's, very few modern log suites exist. Accordingly, high-resolution stratigraphic correlations are difficult. However, we successfully used SP and resistivity log signatures from 105 wells in the field to correlate multiple zones of moderate porosity that appear to be laterally continuous throughout parts of the field. Regions in which log-signature correlations break down are interpreted to correspond to zones of brecciation and fracturing caused

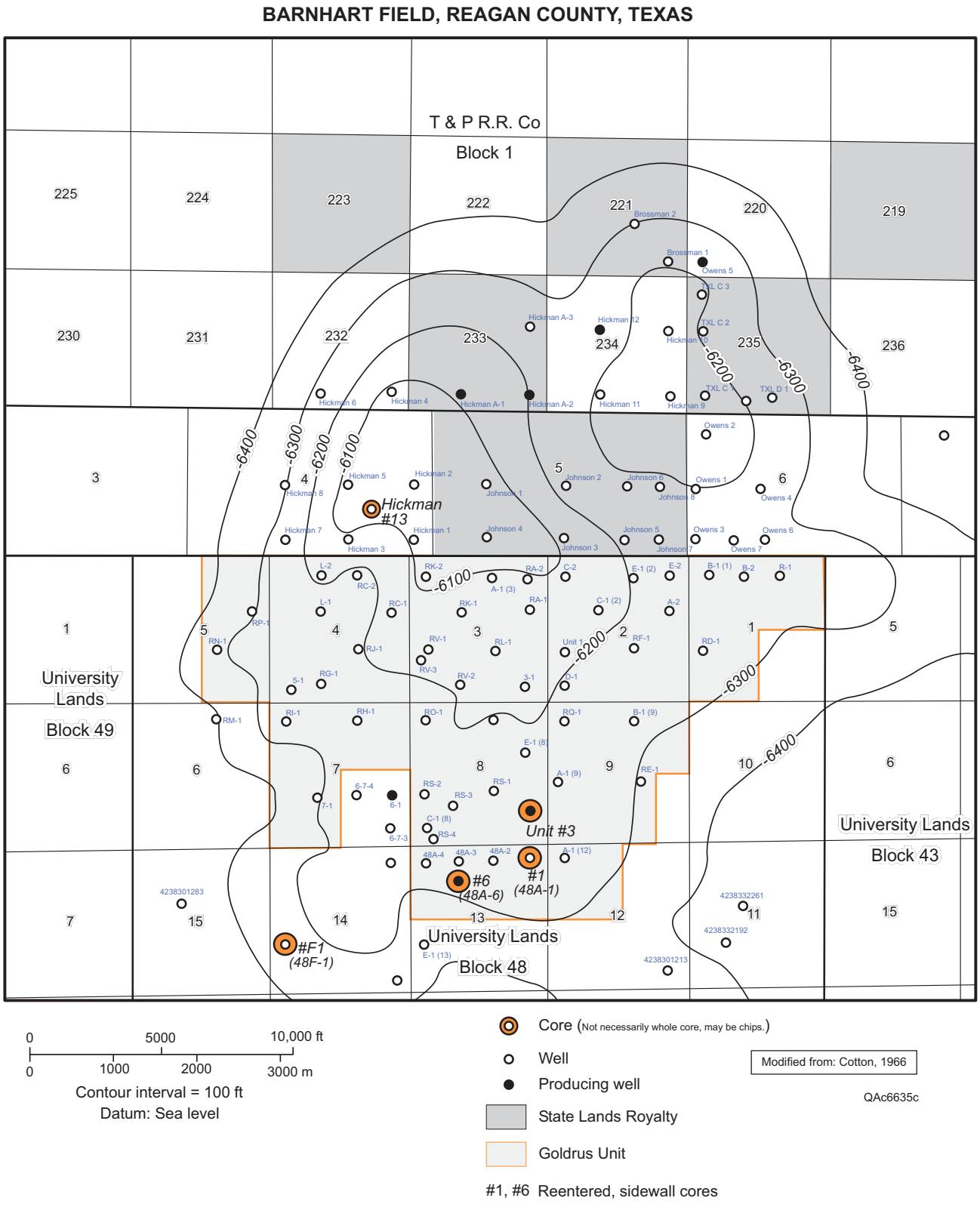

Figure 3. Structure map of Barnhart field.

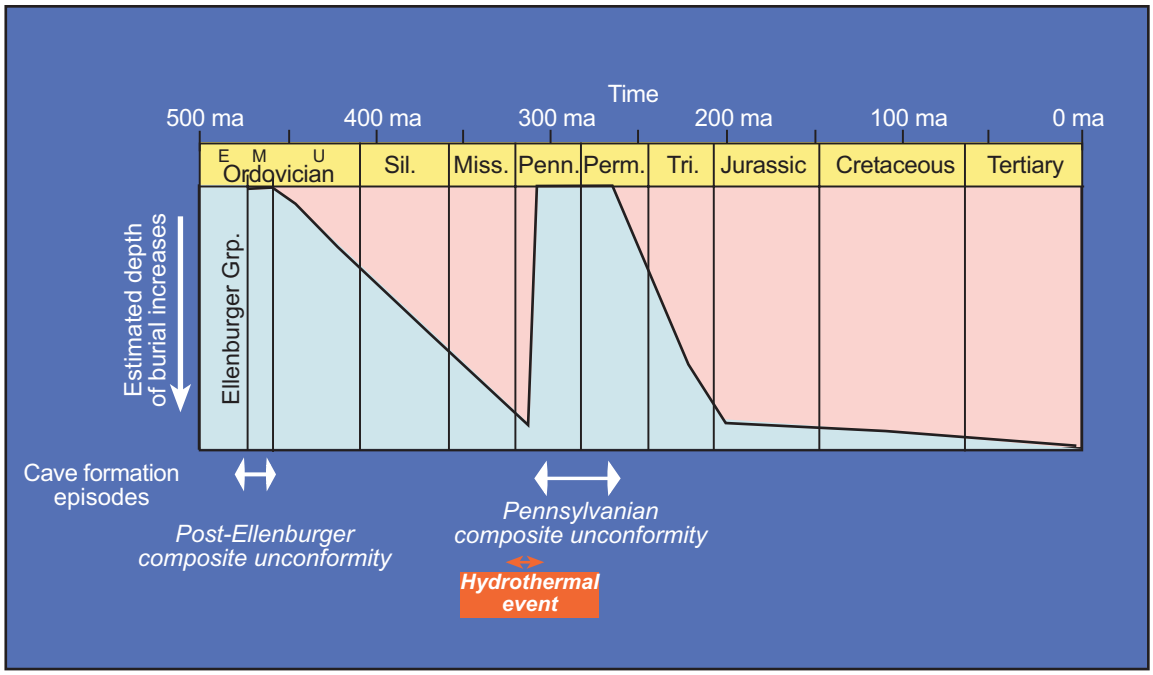

Figure 4. Generalized burial history of the Ellenburger Group in Barnhart field. The Ellenburger Group was exposed to karst processes during Late Ordovician and Pennsylvanian time. During the Early Pennsylvanian time the Ellenburger Group experience hydrothermal processes and tectonic uplift related to the Ouachita Orogeny.

by karsting, strata dissolution (cave formation), and collapse. Recognition that apparent breaks in correlations may define karst and collapse breccias provides a potential basis for the mapping of subsurface karst features.

IV-2. Task 1.0 – Description and Modeling of Field Stratigraphy

The original depositional character of the Ellenburger Group dolomites has been overprinted by karst processes of dissolution and paleocave formation. This overprinting has created a complicated system of original facies, karst features, and fractures that must be differentiated for accurate reservoir modeling and production.

IV-2.1. Subtask 1.1 – Core Description of Facies, Fabrics, and Textures

Goldrus Producing Company provided the project a 41-m (130-ft) core (Goldrus Producing Company Unit #3). The core has been described in detail (Fig. 5) by the following methods: (1) description of fractures before the core was slabbed (presented later under the section on fractures), (2) description of mineralogy and facies of the slabbed core face, and (3) thin-section analysis of diagenesis and pore types.

IV-2.1.1 Mineralogy

The core is completely dolomite except for the interval from 9210 to 9212 ft, which is predominately limestone. Much of the Ellenburger section in the field appears to be dolomite, which is common for Ellenburger producing reservoirs.

IV-2.1.2 Facies

The complete core (Fig. 5) is composed of collapsed paleocave facies. The facies classification by Loucks and Mescher (2001) (Fig. 6) and the breccia/fracture classification by Loucks (1999) (Fig. 7) were used to describe the collapsed paleocave facies. The following paleocave facies have been described (Fig. 5): (1) collapsed ceiling facies; (2) cave-fill, coarse-clast chaotic breccia facies; (3) cave-fill, fine-clast chaotic-breccia facies; and (4) cave-sediment fill facies. The host rock and disturbed host rock facies were not cored in this well, but wireline logs and core photographs from a cored well in another part of the field indicate that these facies may make up much of the field.

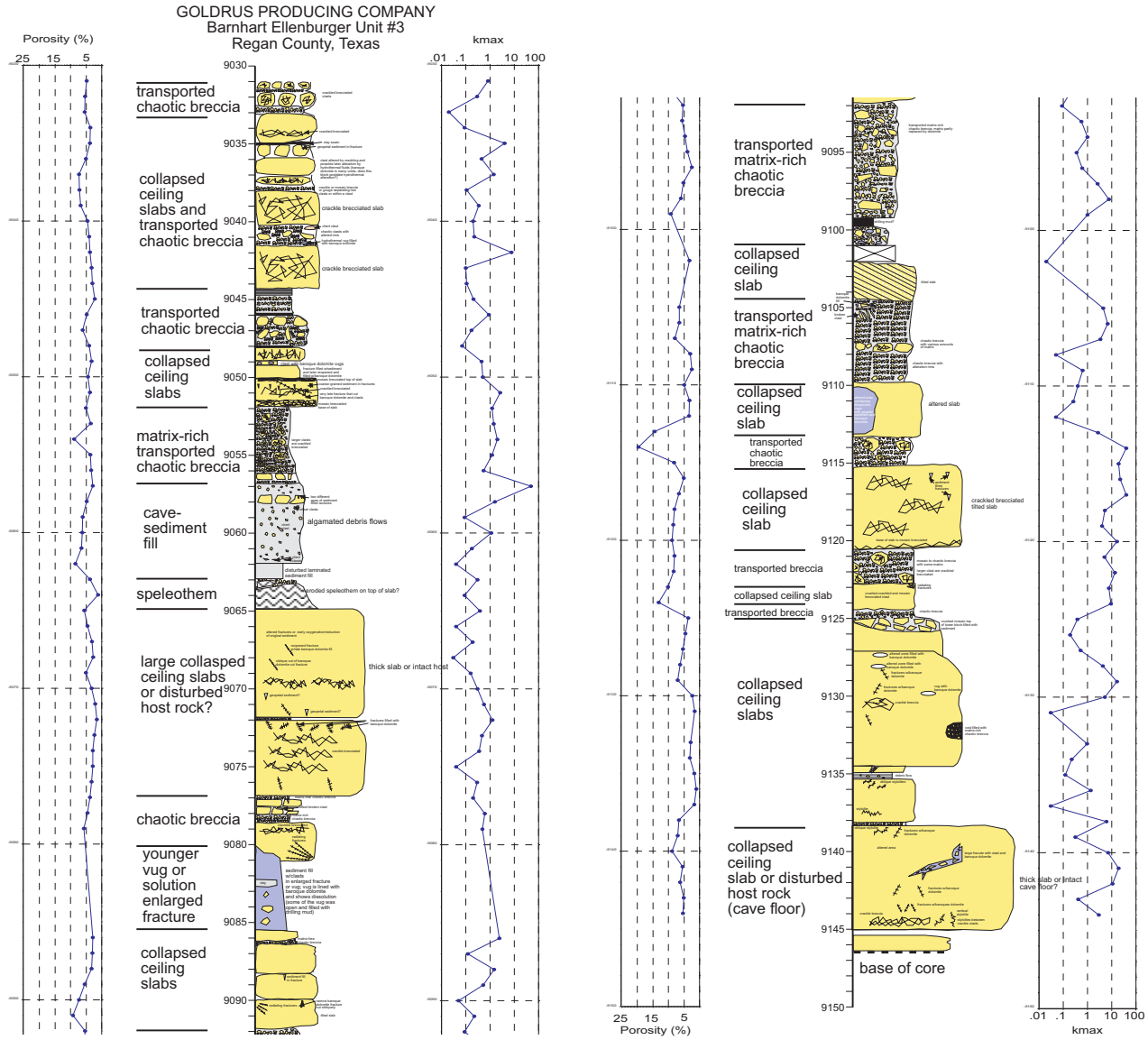

Figure 5. Core description of the Goldrus Producing Company Unit #3 core showing textures and fabrics of the collapsed paleocave system. Photographs of selected core pieces are shown, as well as the whole core porosity and permeability analyses.

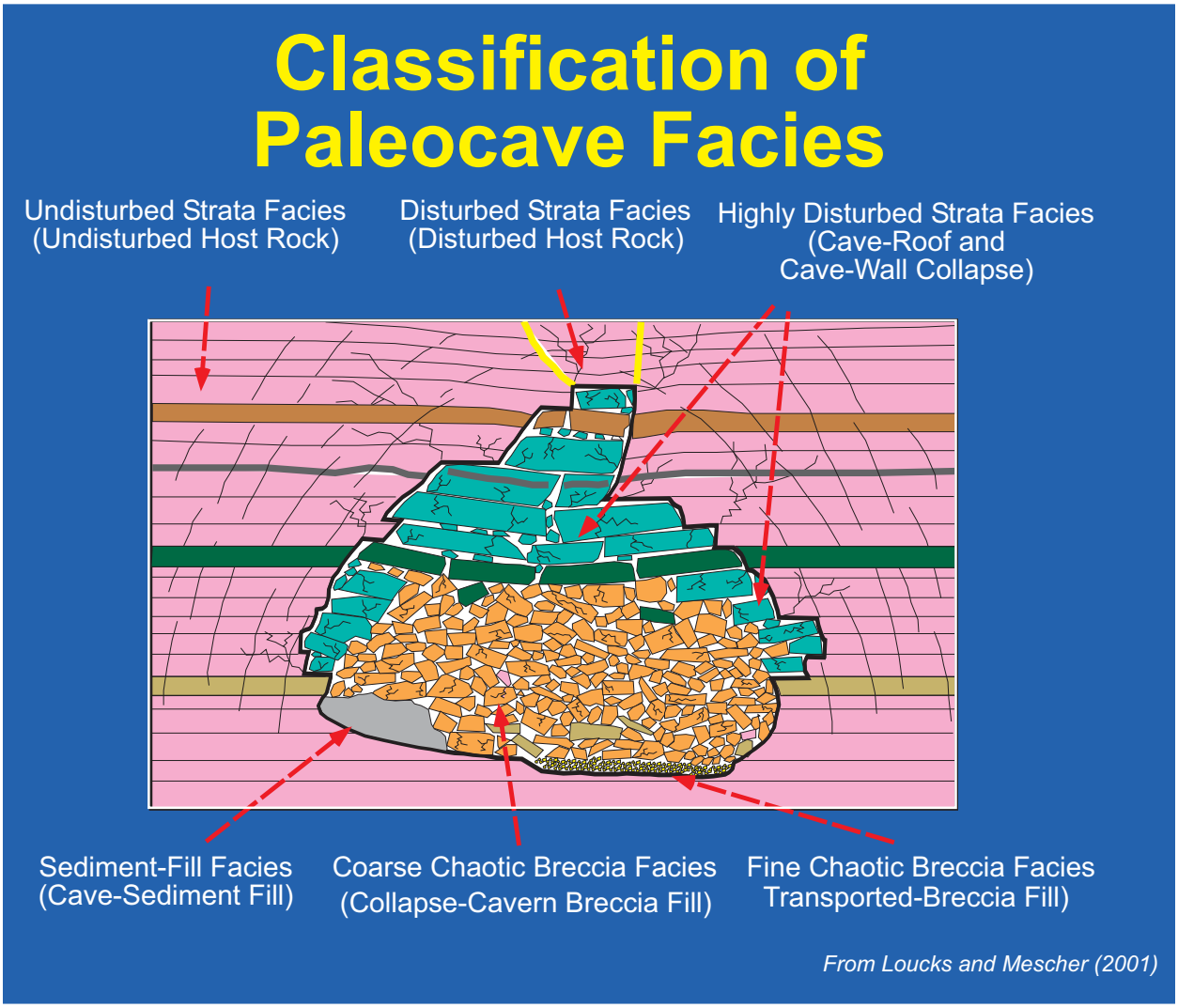

Figure 6. Classification of collapsed paleocave facies. From Loucks and Mescher (2001).

The collapsed cave-ceiling facies is characterized by large blocks and slabs ranging in size (as seen in core) from 35 cm (1 ft) to over 2 m (7 ft). The blocks show that tilting and finer breccia occur between the slabs. The block is crackle-brecciated with some of the brecciated fractures forming pores. The brecciation of the blocks started early in the history of the cave, as indicated by sediment-filled fractures. Other fractures occurred late and are only filled by cement.

The cave-fill, coarse-clast chaotic breccia facies is composed of large blocks that fell from the cave ceiling or walls. They are too large to have been transported and rest where they fell to the

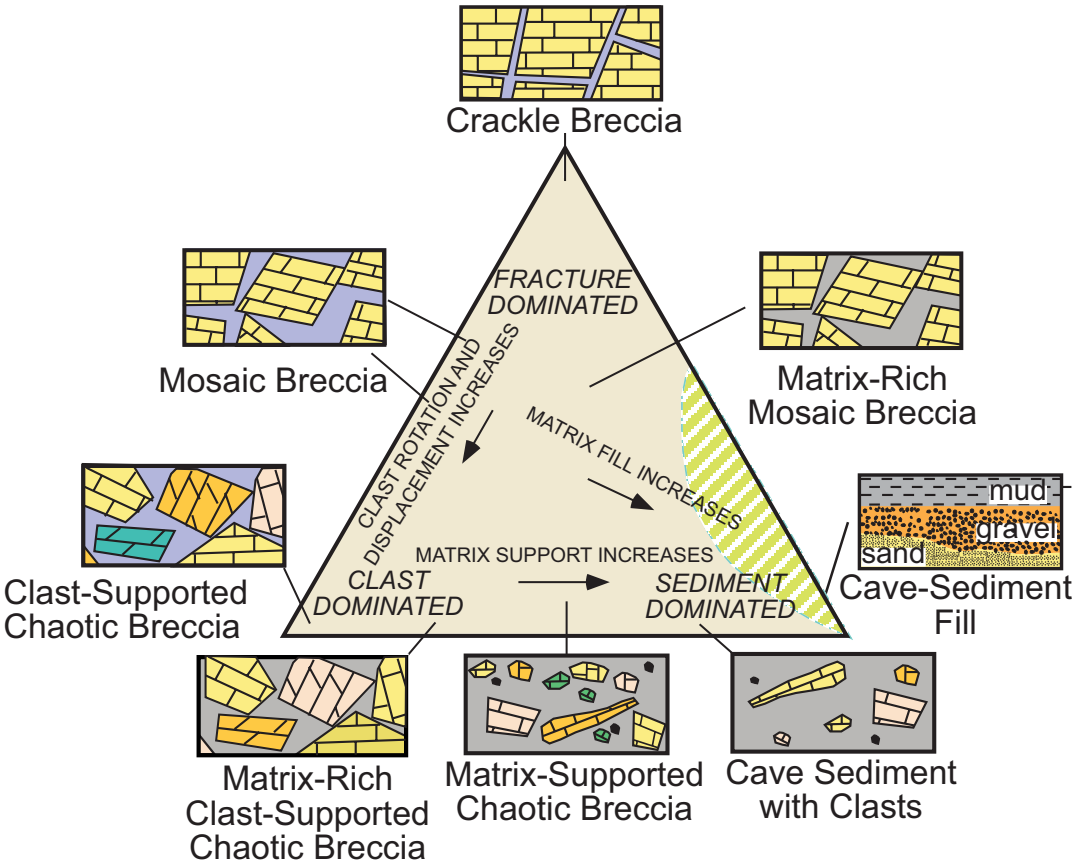

Figure 7. Classification of breccias and cave-sediment fills. Shaded area in the lower right of the diagram indicates that no cave features plot in this area. Cave-sediment fills and breccias can be separated into three end members: crackle breccia, chaotic breccia, and cave-sediment fill. Crackle breccias show slight separation and displacement. Mosaic breccias display some displacement, but they can be fitted back together. Chaotic breccias are composed of displaced clasts that cannot be fitted back together, and they can be composed of clasts of different origins (polymictic). Cave-sediment fill can form a matrix within the breccia, as well as support individual clasts. The best reservoir quality is in the matrix-free breccias. From Loucks (1999).

floor of the cavern. Smaller clasts (generally < 10 cm (~4 inches) characterize the cave-fill, fine-clast chaotic-breccia facies. These chaotic breccias are commonly matrix supported, indicating that they were deposited by debris-flow processes. The cave-sediment fill facies was deposited by suspension processes and is characterized by laminated dolomites. A speleothem occurs at 9663 to 9365 ft.

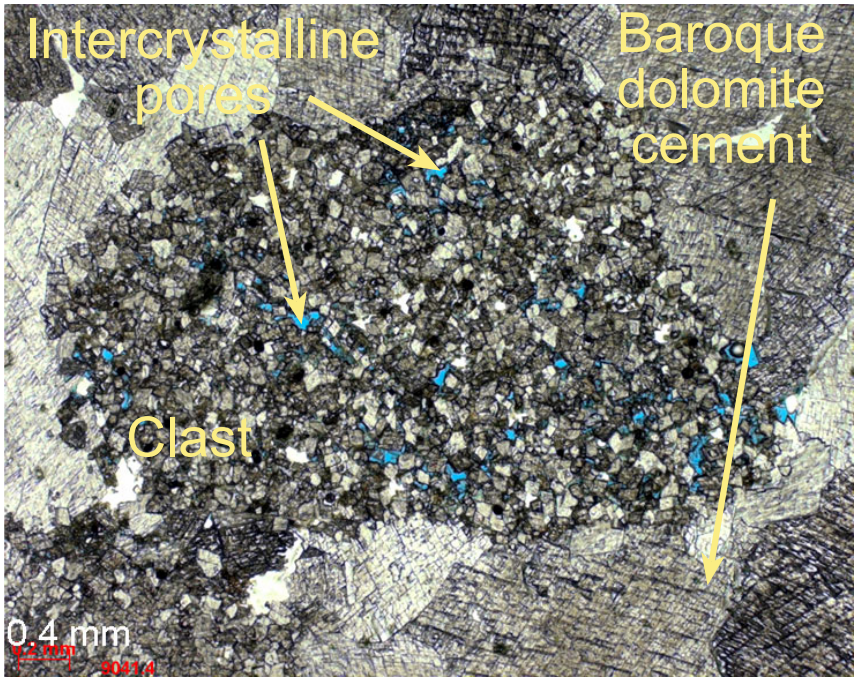

Figure 8. Clast of host rock showing intercrystalline pores.

IV-2.1.3 Pore Types

The pore types noted in the Goldrus Producing Company Unit #3 core consist of (1) original matrix pores in clasts, (2) interclast pores, (3) crackle-breccia pores, (4) mosaic-breccia pores, (5) cave-sediment fill interparticle pores, (6) solution-vug pores, and (7) tectonic fracture pores. The mean porosity within the coalesced collapsed paleocave facies is 4.8% and ranges from 1.2% to 19.7%. The mean permeability is 3.4 md and ranges from 0.02 to 48.2 md. These values are typical of Ellenburger dolomite reservoirs in West Texas (Holtz and Kerans, 1992).

The original matrix pores are only seen in clasts and blocks in the core. Most of the blocks exhibit very low permeability relative to matrix porosity. Figure 8 is an example of a clast of the host rock containing intercrystalline pores. These relationships suggest that the host rock contains layers of this pore type separated by tight layers. Note the wireline-log correlations that are discussed later. Pore types in the porous host rock are assumed to be similar to those seen in the cave-fill clasts. Estimated mean porosity and mean permeability are less than 5% and less than 4 md respectively.

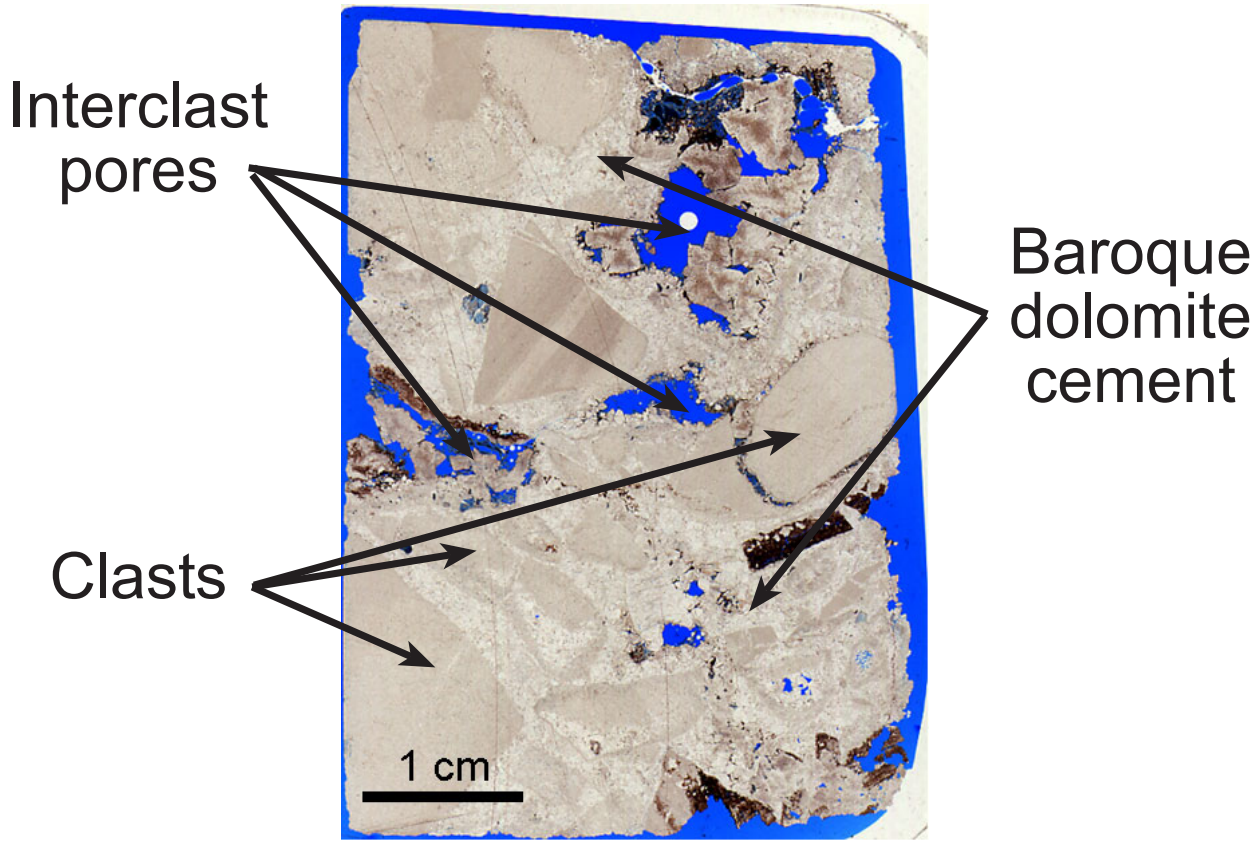

Figure 9. Chaotic breccia with interclast pores. Some of the pore space is occluded by baroque dolomite.

Interclast pores occur between the breccia clasts of matrix-free chaotic breccias. Figure 9 shows a thin section of a chaotic breccia with interclast pores. Baroque dolomite cement has reduced some of the pore space. This type of pore system is limited to the dimensions of the cave void because the origin of the clasts is due to transport in a cavern system. It was noted during the describing of the core that large pore spaces such as these are commonly filled with drilling mud. The drilling mud will affect porosity and permeability analyses, causing them to be lower than if the pores were not filled with drilling mud.

Many of the clasts, slabs, and blocks have crackle-breccia to mosaic-breccia-fracture pores (Fig. 10). These fracture pores are produced by mechanical compaction of clasts, slabs, and blocks. The early-formed fracture pores commonly have detrital carbonate sediment (Fig. 10) in them, whereas later-formed fractures have only cement (Fig. 11). The crackle-breccia fractures are a major pore type, and they are also assumed to be common in the disturbed host rock.

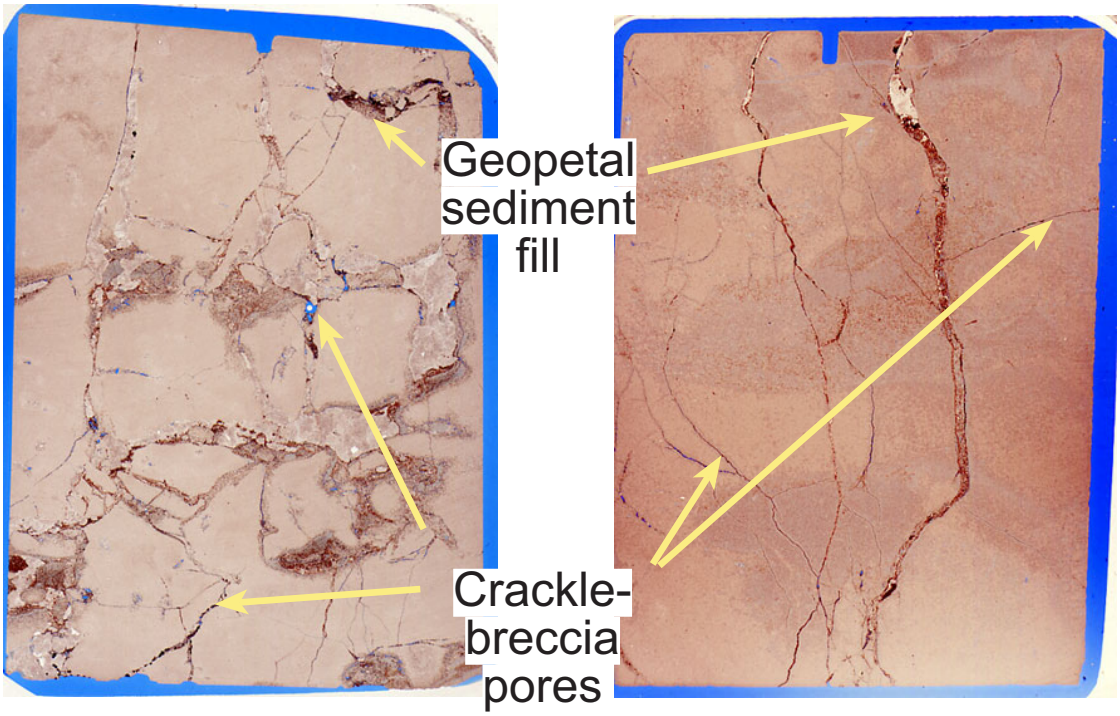

Figure 10. Early-formed, crackle-breccia fracture pores with detrital geopetal sediment. The induced sediment is an early event when water was moving through the former cavern.

The cave sediment fill in this paleocave system contains porosity in the coarser sediment. Figure 12 is a thin section of granular-sized clasts in a larger mosaic breccia. There is some interparticle pore space between the granules; however, much of the pore space is cemented by baroque dolomite. The sand-size detrital carbonate also is slightly porous, but much of the porosity has been occluded by dolomite overgrowths (Fig. 13). The finer sediment is impermeable because the dolomite overgrowths have occluded all the pores.

A macrovug pore is visible in the core at 9080 to 9083 ft (Figs. 14, 15). The full size of the vug cannot be determined from the core or from the image log, but it is at least 1 m (3 ft) high. It could be a solution cavity or a solution-enlarged fracture. The image log (Fig. 15) displays the best view of the macrovug. The vug has a small amount of detrital clay, indicating that the vug was open near the surface. During drilling, much of the vug was packed with drilling mud.

Some late through-going fractures are noted in the core (Fig. 16). The fractures cut a well-lithified breccia and cement, indicating that their origin postdates brecciation and baroque dolomite

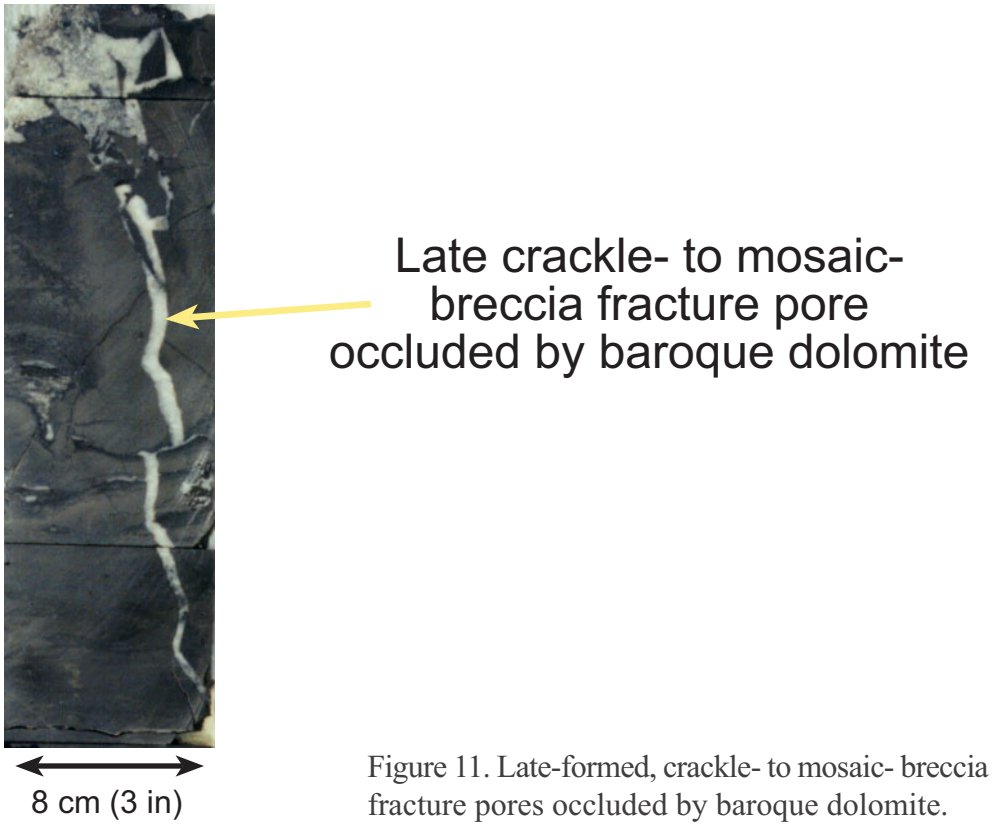

Figure 11. Late-formed, crackle- to mosaic- breccia fracture pores occluded by baroque dolomite.

cementation. The baroque dolomite is assumed to be associated with the Pennsylvanian Ouachita Orogeny; therefore, the fractures must be Pennsylvanian or later in age. Cement occludes the fracture pores; however, other fractures related to this period of deformation may be open. The origin of the fractures is not clear. They may be related to tectonic stresses during the uplift and reburial of the Ellenburger section, or they may be related to mechanical compaction of large blocks with burial.

IV-2.2. Subtask 1.2 – Calibration of Wireline Logs

The collapsed paleocave facies described in the Goldrus Producing Company Unit #3 core have been calibrated to the wireline and image logs. This calibration has produced a collapsed-paleocave type-log section (Fig. 17) that allows the recognition of nonhost rock sections. Combining this type-log section with other correlation techniques aids in defining the distribution of karsted sections in the Barnhart reservoir, which is discussed more under Subtask 1.3.

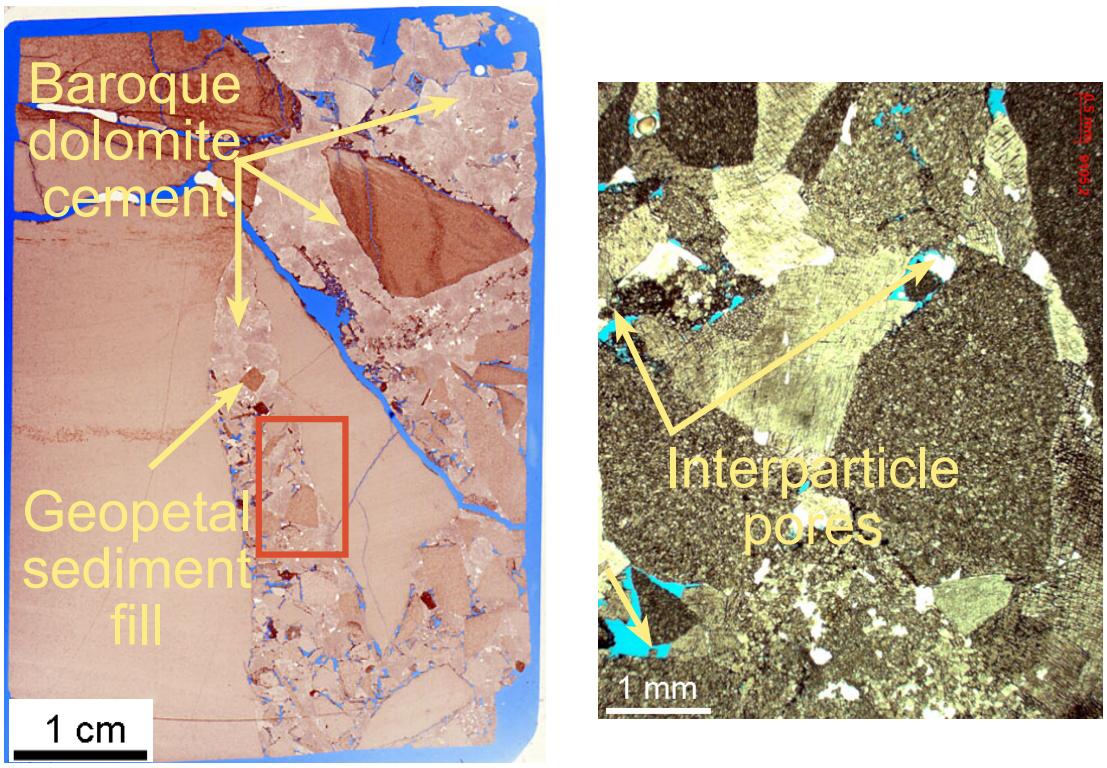

Figure 12. Interparticle pores between granules in a mosaic breccia.

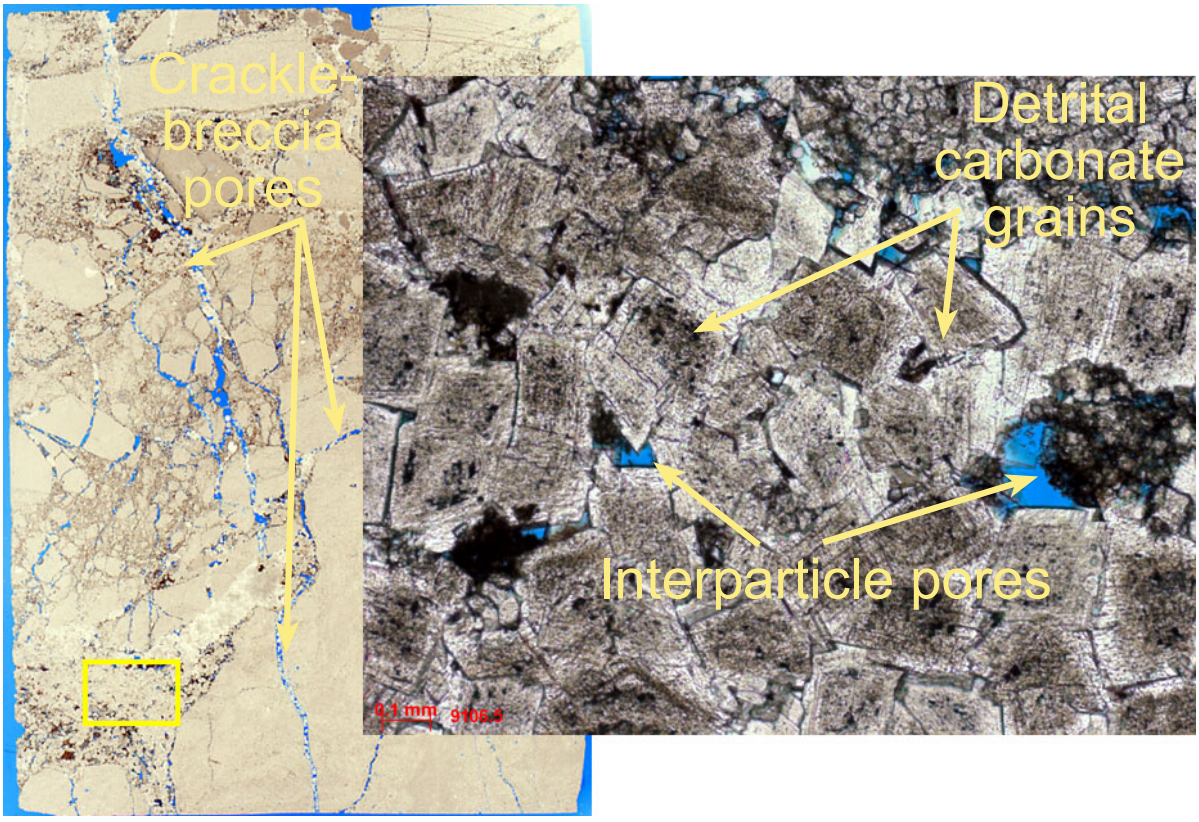

Figure 13. Interparticle pores between sand-sized detrital carbonate that has dolomite overgrowths.

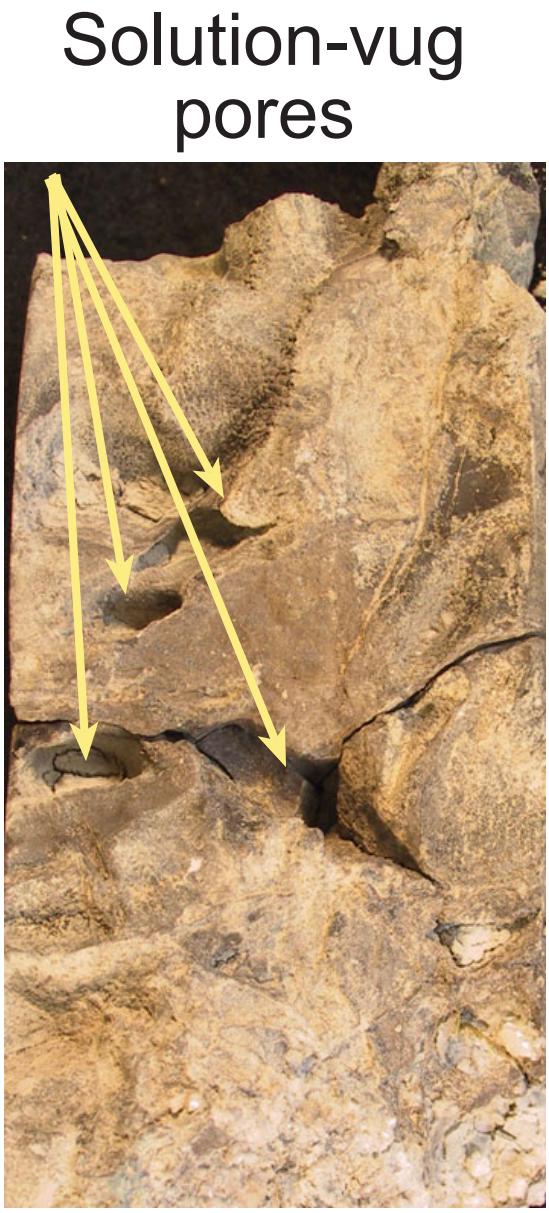

Figure 14. Core slab photograph of the side of a macrovug showing a solution-etched surface.

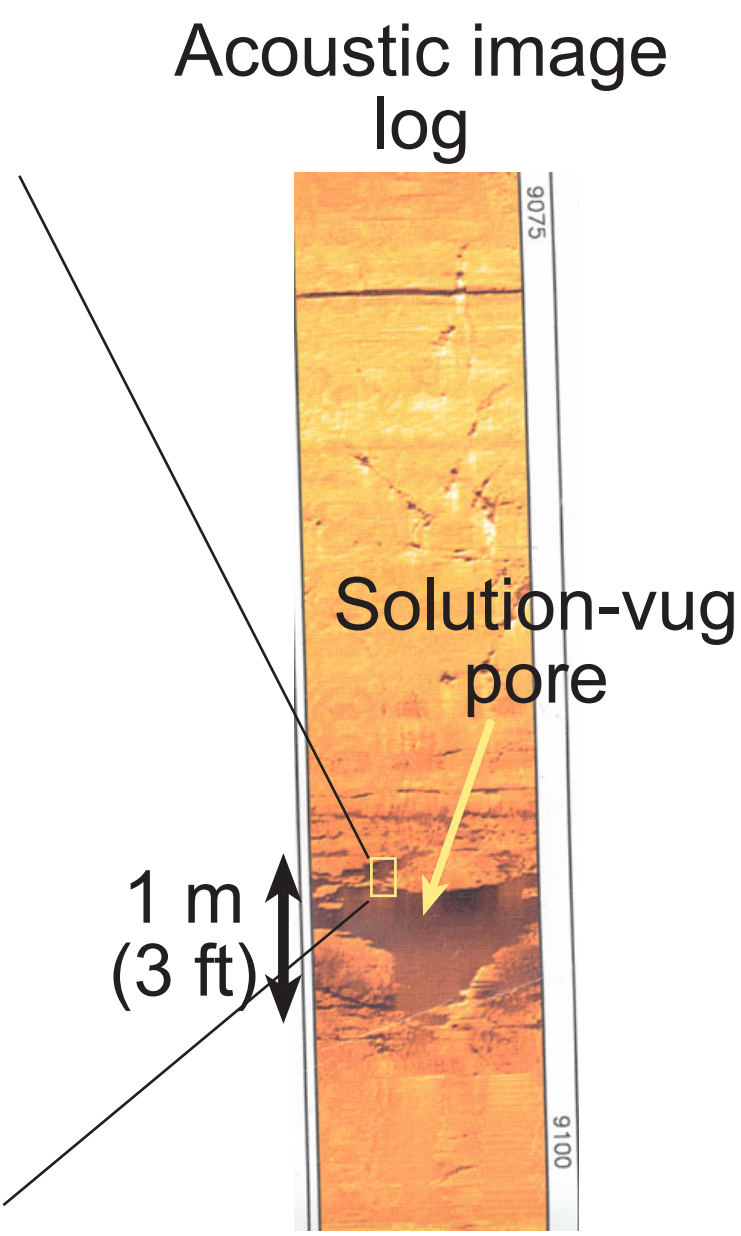

Figure 15. Image log view of the solution macrovug.

IV-2.3. Subtask 1.3 – Establishment of Stratigraphic Architecture

A series of wireline cross sections are being prepared. Preliminary correlations throughout the field (105 wells) are complete. We are now refining the wireline cross sections using Landmark's Stratworks correlation program. We are trying to define the distribution of the porous zones in the

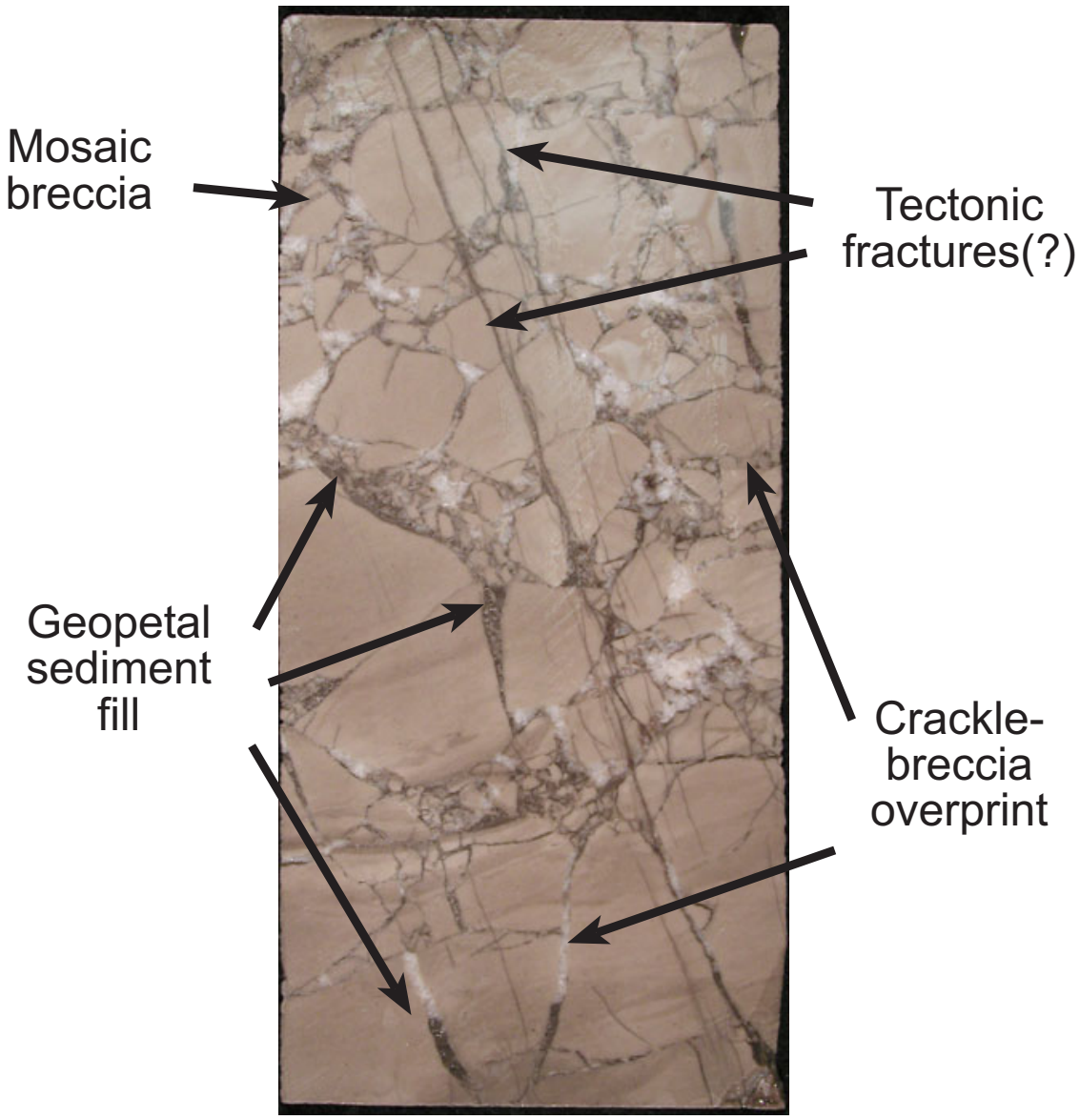

Figure 16. Through-going fractures that cut lithified breccia clasts and baroque dolomite cement.

host rock and map the distribution of the collapsed paleocave deposits. Correlations are difficult because of the age and types of wireline logs available (primarily SP and resistivity) and the lack of contrasting mineralogies (e.g., dolomite versus terrigenous clay) or facies. Figure 18 is a cross section showing the apparent continuity of porous and nonporous zones in the host rock and the loss of continuity in a collapsed paleocave zone.

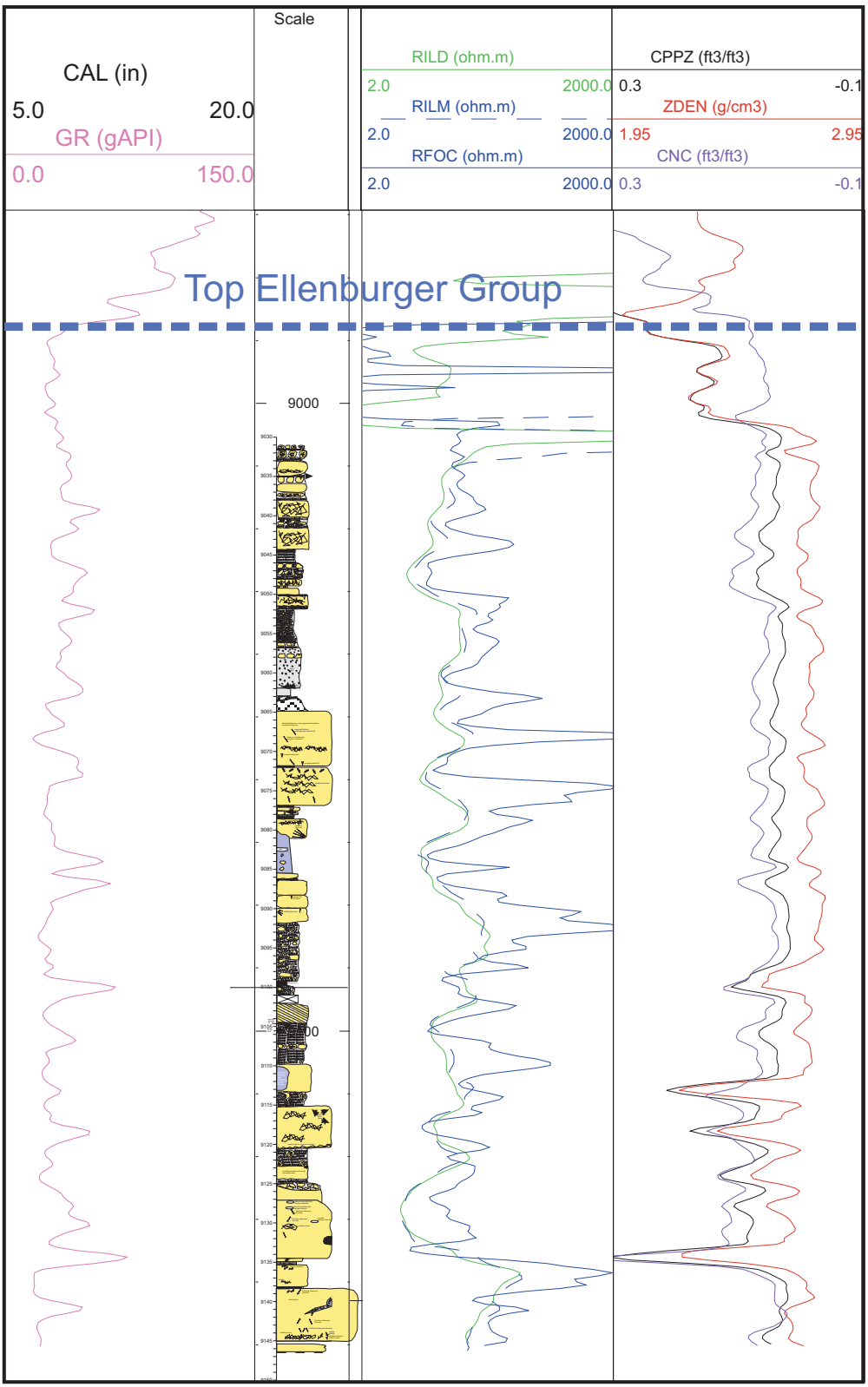

Figure 17. Goldrus Producing Company Unit #3 core has been calibrated to the wireline and image logs. This calibration has produced a collapsed-paleocave type-log section that allows the recognition of nonhost rock sections.

B

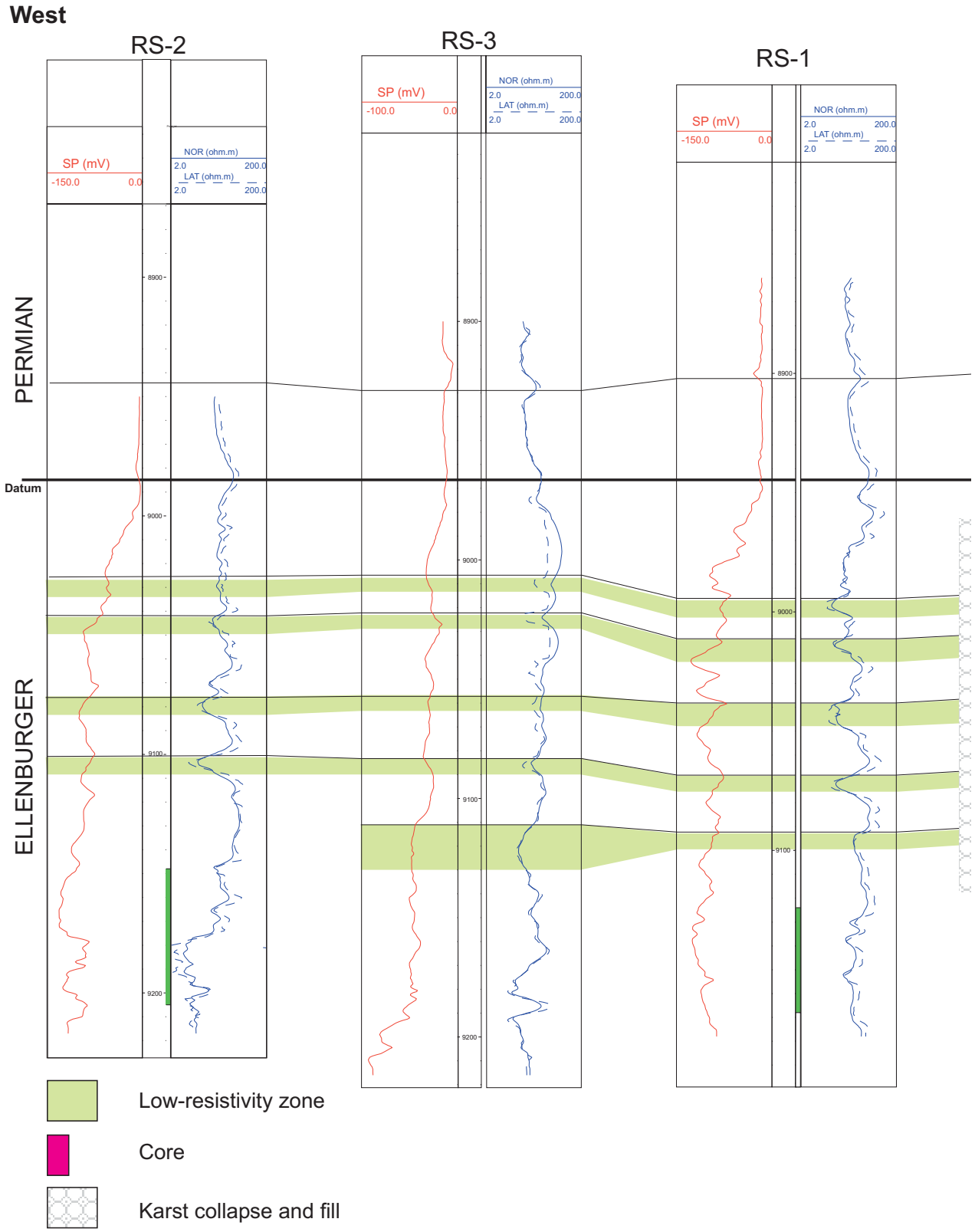

Figure 18. Example of a wireline-log cross section from Barnhart field. Correlations are generally flat and parallel except where the stratigraphic section has been affected by karsting.

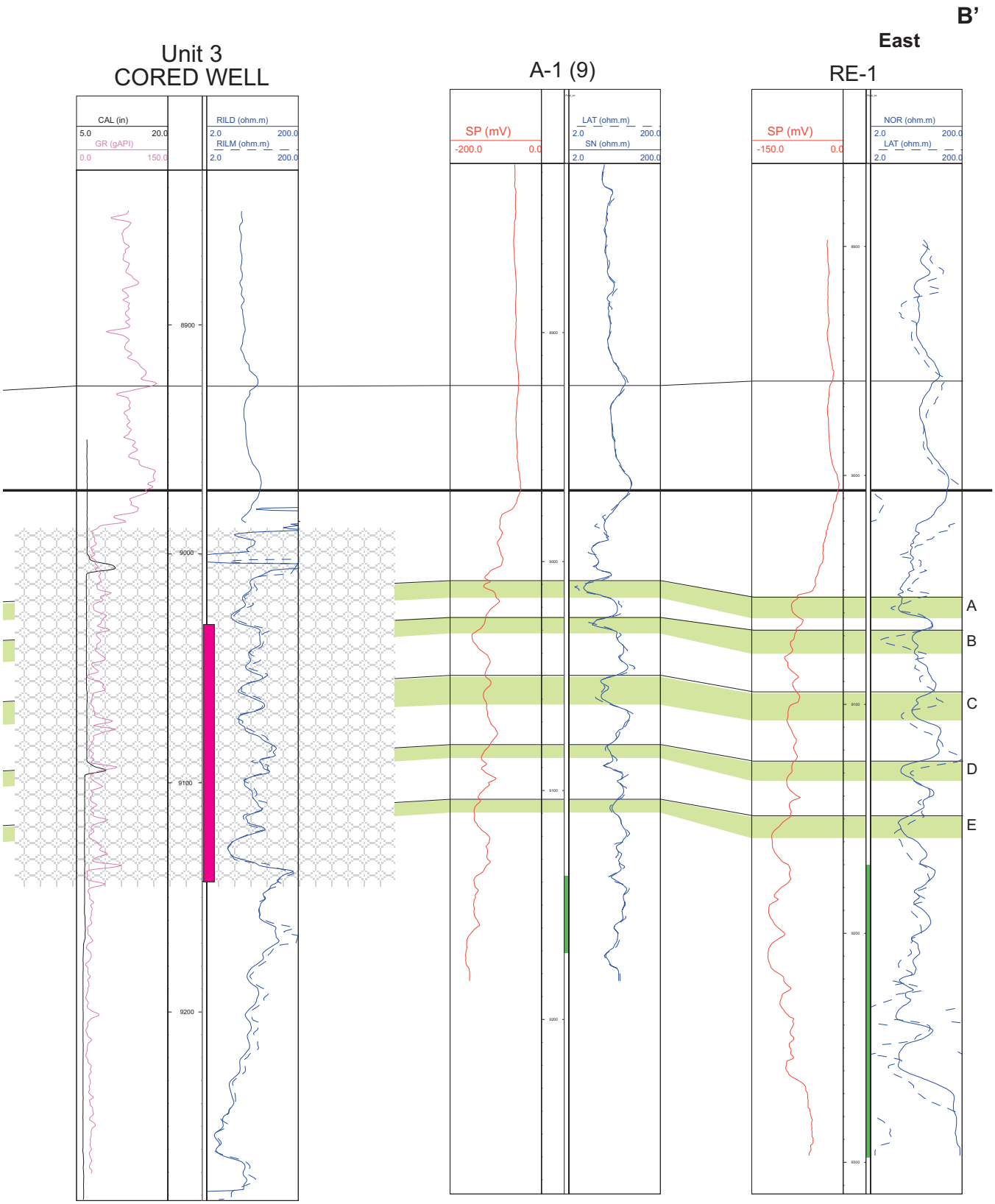
B'
East
Unit 3
CORED WELL
A-1 (9)
RE-1
CAL (in)
5.0
20.0
GR (gAPI)
0.0
150.0
RILD (ohm.m)
2.0
200.0
RILM (ohm.m)
2.0
200.0
SP (mV)
-200.0
0.0
LAT (ohm.m)
2.0
200.0
SN (ohm.m)
2.0
200.0
SP (mV)
-150.0
0.0
NOR (ohm.m)
2.0
200.0
LAT (ohm.m)
2.0
200.0
8900
9000
9100
9200
A
B
C
D
E

IV-3. Task 2.0 – Characterization and Modeling of Matrix Petrophysical Properties

We will combine available core-analysis data with wireline-log data to characterize the matrix porosity and permeability of the Ellenburger reservoir. With these data we will construct a simple 3-D reservoir model to serve as a basis for modeling of OOIP and HPAI injection response.

Core analysis data are only available from two wells: (1) Goldrus Producing Company Unit #3 and (2) Belco Hickman #13. Also, a few modern log suites exist in the field from which porosity measurements can be calculated. Another core and several modern log suites will be obtained this summer as more drilling takes place and these data will be integrated into the data set.

IV-4. Task 3.0 – Characterization of Fractures

On the basis of our early studies of cores and image logs from the Ellenburger at Barnhart field, we have concluded that fractures are abundant in the reservoir (Gomez and others, 2001). These studies define two fracture orientations in the field. Early models suggested that these fractures were entirely of tectonic origin, but more recent work (Combs and others, 2003; Loucks and Combs, 2003) show that they are in part associated with karst processes (cave formation and collapse). Because these two types of fractures may have very different fluid flow characteristics, differentiation of the two types of fractures is critical for accurate reservoir modeling. We will integrate our studies of fractures and karst features to develop methods of defining the distribution and characteristics of each fracture type.

IV-4.1. Subtask 3.1 – Characterization and Differentiation of Fracture Types

Much effort is being put into defining the origin of fractures because fractures of different origins can have vastly contrasting lateral and vertical distributions. Therefore, it is important to understand the quantity of collapsed-paleocave-induced fractures versus tectonic-induced fractures. At present, the only whole core (not core plugs) we have to study is the Goldrus Producing Company Unit #3 core, and it contains only the collapse paleocave facies. In this core, it is difficult to document tectonic fractures. Goldrus Producing Company is planning to obtain another core this summer

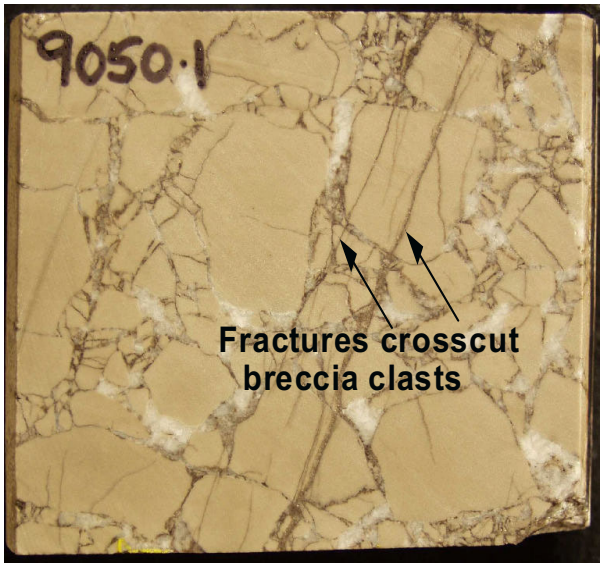

Figure 19. Slab face of Goldrus Producing Company Unit #3 core from 9050.1-ft depth. Fractures crosscut multiple clasts and late baroque dolomite cement (white). Core slab is 4 inches wide.

from what may be the host-rock facies. This core will provide us more information on possible tectonic fractures.

IV-4.1.1 Collapse Paleocave Associate Fractures

These fractures were discussed in the section earlier on pore types (IV.2.1). The fractures are predominantly crackle-breccia fractures. Many of the fractures are open and only slightly occluded with cement (mainly baroque dolomite).

IV-4.1.2 Tectonic Associate Fractures

In whole core from the Unit #3 well, fractures several tens of centimeters long that crosscut lithified breccia and baroque dolomite were observed (Figs. 16, 19). The postbrecciation fractures have two approximately orthogonal trends, but the orientation of individual fractures, or groups of fractures in the same portion of core, is not determinable because the core is unoriented. We attempted to use the image log to orient the core, but this proved impossible for all but the top 10 m (30 ft) of

core, which has dominantly NW-trending, postbrecciation fractures. In this study we are attempting to quantify the fracture intensity and sealing characteristics of postbreccia fractures.

IV-4.1.2.1 Methods

Our goal was to quantify the fracture intensity and sealing characteristics of postbreccia fractures. To do so we used microfractures in sidewall cores from A1 and A6 wells and in samples from the Unit #3 core in Barnhart field. The use of microfractures allows us to collect a large enough population to make predictions about large, potentially open fractures that were not sampled by the sidewall cores or whole core and which probably populate the host rock in the interwell volume. The underlying principles for this approach were outlined by Laubach and others (2000).

Opening-mode-fracture, aperture-size measurements were collected for a NE-trending fracture set from oriented sidewall cores in the A1 well from depths of 9055 and 9087 ft and from the dominant set in samples from the Unit #3 well at 9070 ft and 9079 ft. Microfractures were measured using image mosaics collected on a scanning electron microscope with a cathodoluminescence detector for the A1 well samples and for the Unit #3 9070-ft sample. The detectors and processing used for these images record CL emissions in the range of ultraviolet through visible into near infrared and convert them to gray-scale intensity values. All images were acquired using an Oxford Instruments MonoCL2 system attached to a Philips XL30 SEM operating at 15 kV. For the 9079-ft Unit #3 sample, the image mosaic was collected using cathodoluminescence on a transmitted light microscope.

Microstructures were imaged on polished thin sections cut parallel to bedding. Scanned CL photographs were taken in traverses several millimeters in length and stitched electronically into mosaics. Typically a mosaic of 30 to 40 individual images at a scale of 1:150 is required to record a continuous CL image along the short side of a 2.65by 5.3 cm (1 by 2 inches) thin section. To increase the likelihood of intersecting microfractures genetically related and parallel to macrofractures, mosaics were oriented perpendicular to known macrofracture strike. An example of a portion of an image mosaic is shown in Figure 20. Different dolomite cements and calcite

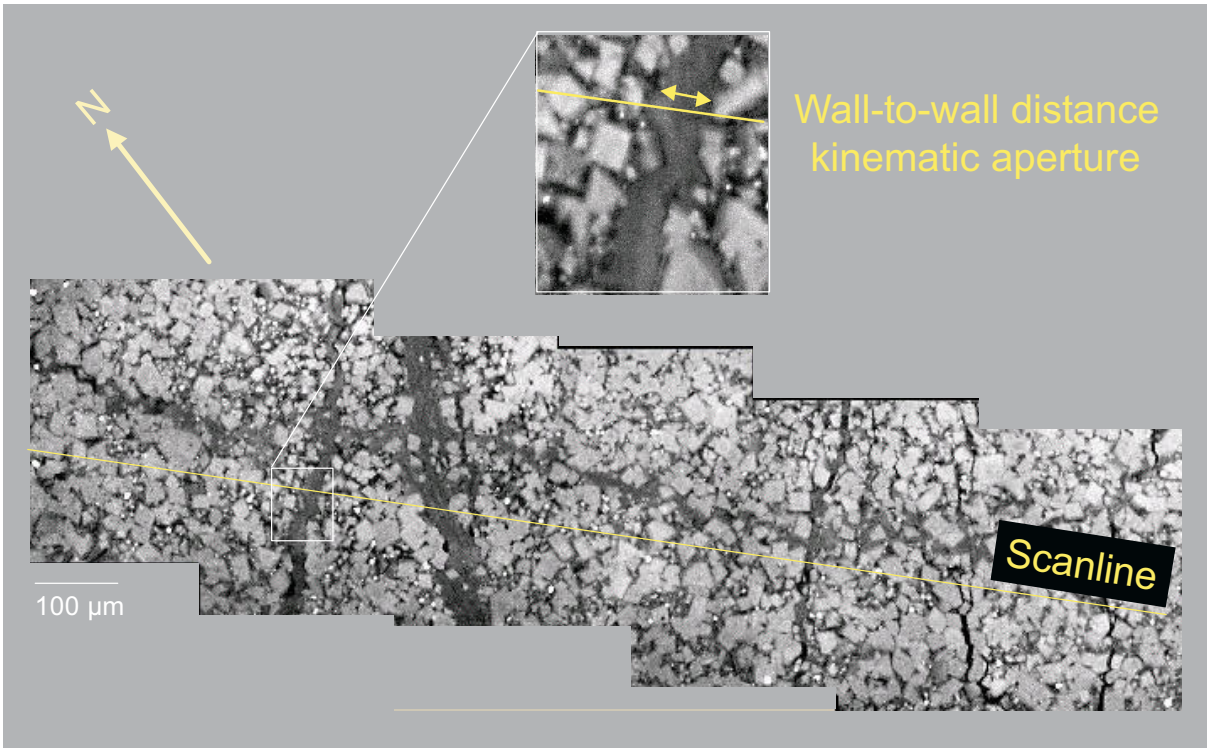

Figure 20. SEM-CL image mosaic of fractures from the A1 well sidewall core at 9055-ft depth. Fracture apertures for the NE-trending set were measured along a scanline for a 1-D analysis.

cements are distinguished on the basis of degree and type of luminescence (Reed and Milliken, 2003) and by using secondary electron images of the same area. Orientation and size were mapped electronically using commercially available software (Canvas 5.0) by defining four points—the two fracture tips and two opposite points on the fracture walls at the widest aperture. Fracture attributes were measured and compiled using in-house software that uses the digitized parts of the four points to calculate length, aperture, and orientation (Ortega, 2002). The area of the CL mosaic is also calculated using image-processing software.

Kinematic apertures of opening-mode fractures were measured along scanlines normal to fracture strike for one-dimensional analysis. Maximum kinematic apertures of fractures within a mosaic area were measured for two-dimensional analysis. Kinematic aperture is the wall-to-wall distance normal to the fracture and is independent of whether the fracture is open. Aperture data are presented on cumulative frequency plots of fracture apertures, normalized to scanline length or area (Fig. 21).

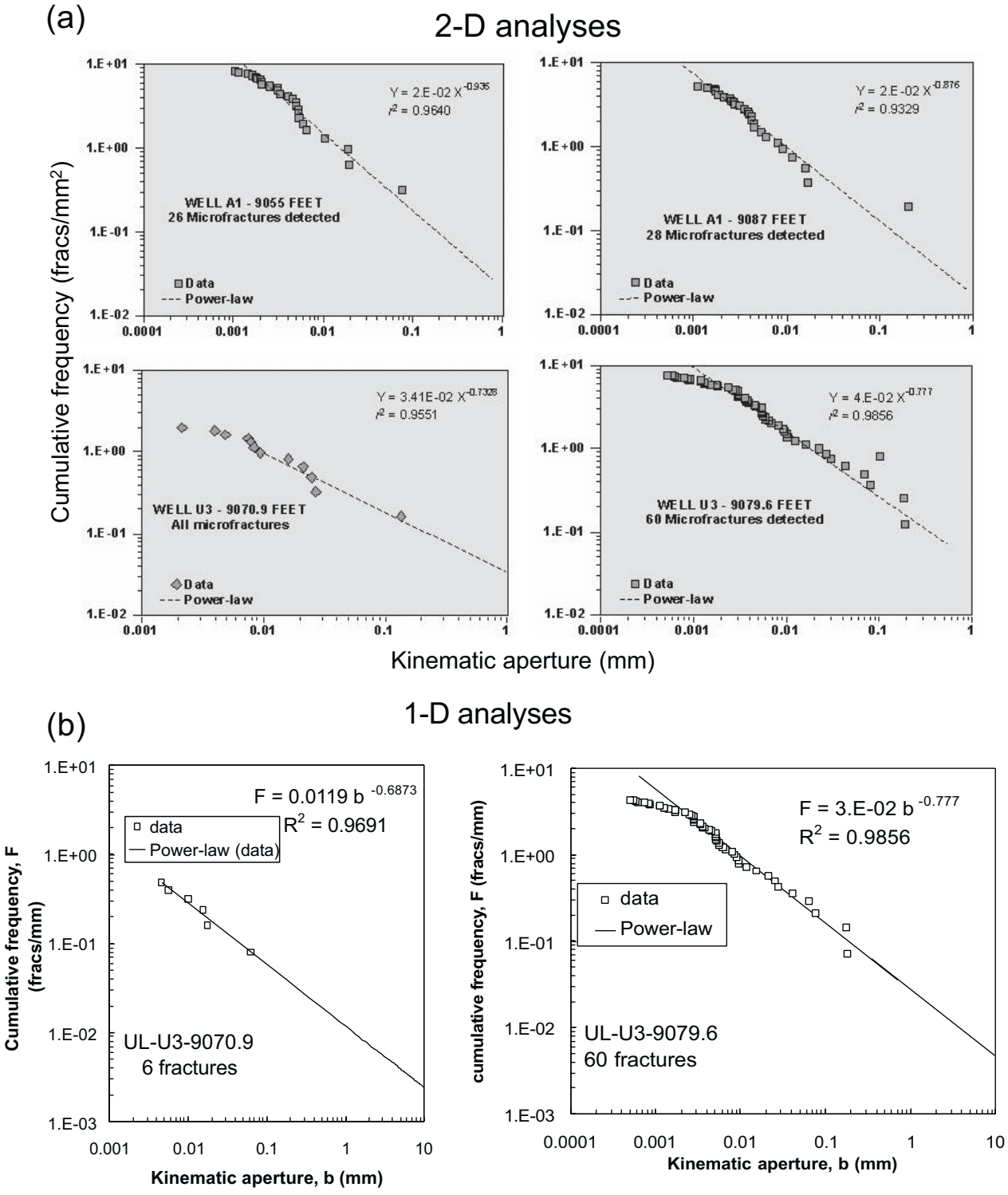

Figure 21. Aperture-size distribution cumulative-frequency plots. Data are fit to a function that models truncation and censoring at either end of the data set as well as a power law (straight line on a log-log plot) for the main part of the data. Only the power law is shown, but the correlation coefficient applies to the whole function. (a) 2-D data from A1 well, 9055- and 9087-ft depths and the Unit #3 well, 9070.9- and 9079.6-ft depths. (b) 1-D data for Unit #3 well from 9070.9- and 9079.6-ft depths.

The data are fit to a power-law function of the form F = ab-c, where F is cumulative fracture frequency, a is the coefficient, b is the fracture aperture, and c is the exponent of the power-law relationship. Where these parameters can be delineated for microfracture size distributions, the equations can be used to predict the distribution of sizes of macrofractures in the same volume of rock (Marrett, 1996). Power-law distribution coefficients may be thought of as a measure of fracture intensity at a given size. For example, if b = 1, then the equation simplifies to F = a. Exponents reflect the slope of the power law on a log-log plot. The data show departures from a power-law function at high and low ends of the measured size range. These are recognized as truncation and censoring sampling artifacts (Marrett and others, 1999).

IV-4.1.2.2 Fracture Intensity Results

The utility of the cumulative frequency plots is that the power law may be extrapolated to give a measure of predicted fracture intensity, in terms of the number of fractures per unit length of scanline, for any given aperture size. Typically in dolomites fracture porosity may be found in submillimeter-wide fractures, but for fractures to be effective conduits for fluid flow they probably need to be at least 1mm wide. The power law is extrapolated to aperture sizes of up to 1 mm (Fig. 21a) and 10 mm (Fig. 21b).

Fracture intensity must be reported in reference to the fracture aperture being considered. Here, fracture intensities are reported for fractures ≥1 mm wide. For the 2-D A1 well samples from depths of 9087 ft and 9087 ft, intensity was 0.018 and 0.02 fractures/ mm^2 respectively. For the 2-D Unit #3 well analyses for samples from depths of 9070.9 ft and 9079.6 ft, intensity was 0.034 and 0.04 fractures/ mm^2 respectively (Fig. 21a). For 1-D analysis using a scanline rather than a mosaic area to collect the fracture aperture data, the Unit #3 samples yielded intensities of 0.012 and 0.03 fractures /mm, for fractures ≥1 mm wide (Fig. 21b).

Fracture intensities from different samples may be compared. Fracture intensity for the NE-trending set at different depths in the A1 well was not significantly different, suggesting that for those depths tested, the opening-mode fracture response was similar. Intensities measured in the

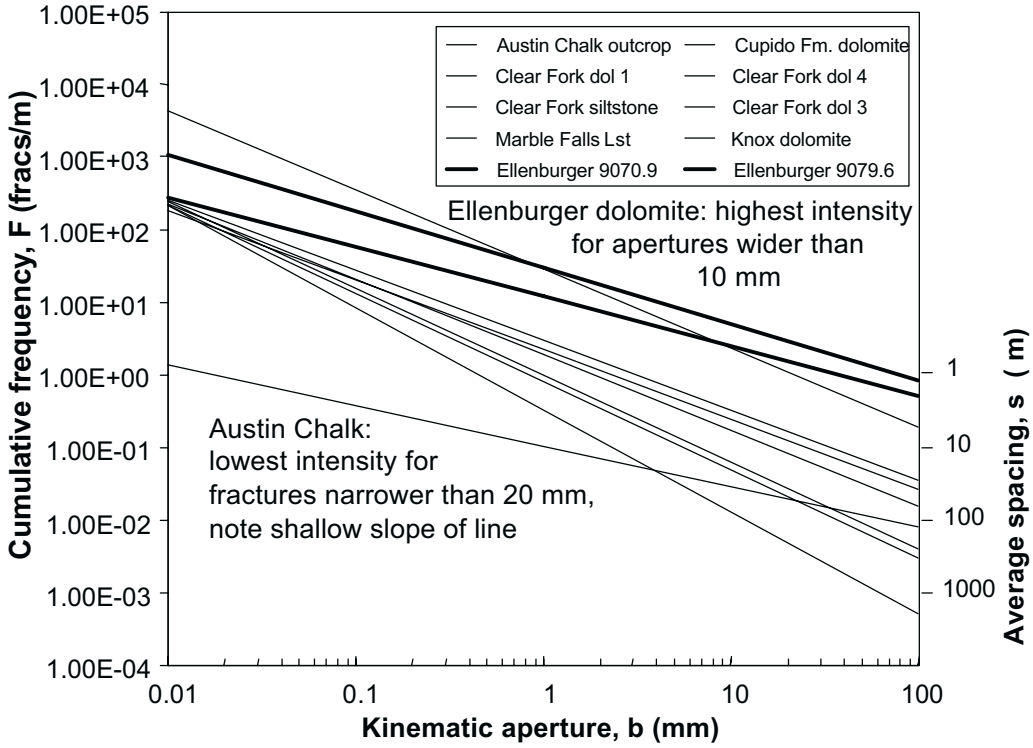

Figure 22. Cumulative-frequency plot for 1-D aperture-size distributions of various carbonates. The samples from 9070.9 ft and 9079.6 ft from the Unit #3 well (individual plots in Fig. 3) are shown relative to other carbonates (heavy lines). They plot near the top of the range of curves, indicating that fracture intensity is relatively high in the Unit #3 well.

Unit #3 well were slightly higher than those in the A1 well. In the Unit #3 well, the opening-mode fracture intensity is also high relative to most other fractured carbonates we have measured (Fig. 22). The inverse of cumulative frequency (fractures/meter) is average fracture spacing (meters/fracture). Although fractures are generally not evenly spaced and tend to be clustered, we use the average spacing measure as an alternative way to represent fracture intensity. In the Unit #3 well fractures with kinematic apertures (wall-to-wall distance across fracture, irrespective of fill) of 10 cm (~ 4 inches) are predicted to be spaced 2 to 5 m (6 to 15 ft) apart.

Further SEM-CL image mosaics have been collected for the NW-trending fracture set in samples from the A1 well. These mosaics will be used to collect aperture size distribution data, which will allow us to assess the fracture intensity for the NW-trending set of fractures in this well relative to each other and to the intensities for the NE-trending set. Preliminary crosscutting observations of fractures in the two sets are inconclusive, and it may be that the two sets are broadly contemporaneous.

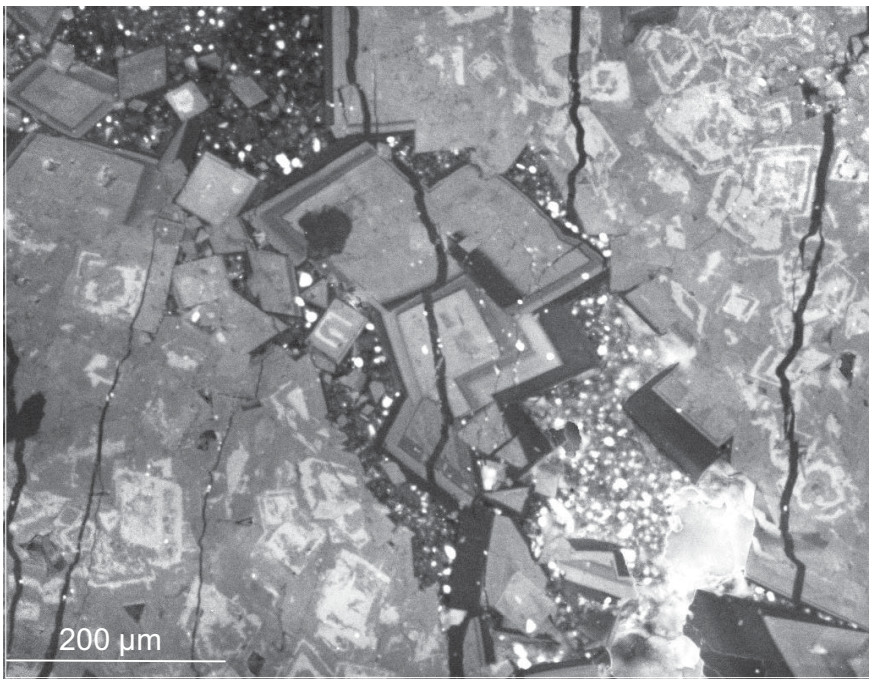

Figure 23. Fractures sealed with low-luminescence cement follow internal and external rhombohedral dolomite crystal boundaries, indicating the rock was dolomitized prior to fracture propagation. Also note zoning of the host-rock dolomite. The external zones are also low-luminescence dolomite, which precipitated in the host rock at the same time as in the fractures.

IV-4.1.2.3 Fracture Timing and Sealing Results

Principles of fracture sealing mechanisms were discussed fully by Laubach (2003). Fracture sealing takes place by two different processes, one synchronous with fracture opening (synkinematic), the other postdating the opening event (postkinematic). The question of whether a fracture will remain open in the subsurface depends upon the operation of both processes. The first sealing process tends to seal the smallest fractures in a population but leaves the larger fractures open. The second process may completely occlude remaining porosity in the large fractures.

Scanning electron microscope-based cathodoluminescence (SEM/CL) allows the detection of microfractures that otherwise would remain invisible because of their small size and because the cement precipitated in them is in optical continuity with crystals in the wall rock. SEM/CL revealed that fractures formed after a phase of dolomite replacement because fractures have a distinct morphology, indicating that they grew initially by propagation along rhombohedral dolomite-grain boundaries (Fig. 23).

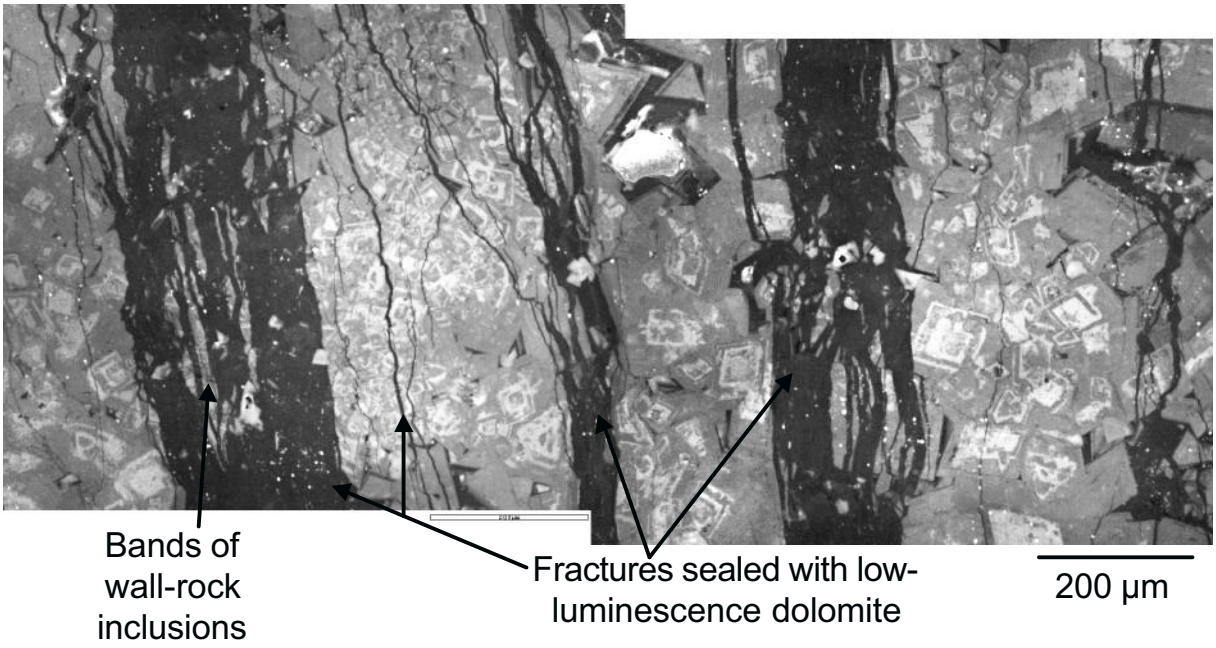

Figure 24. Crack-seal structure in fractures from the Unit #3 well at 9079.6-ft depth. Fractures are sealed with low-luminescence dolomite (black). In each fracture there are bands of wall rock inclusions entrained within the fracture as a result of multiple opening events. Some of these inclusions have the dolomite zoning in the host rock preserved.

A low-luminescence dolomite cement precipitated during fracturing (synkinematic) and formed cement bridges and a fracture lining. Evidence of synkinematic cement is provided by the presence of crack-seal structure (Fig. 24). Fractures repeatedly open and seal with cement of the same composition, producing bands of wall rock and/or fluid inclusions within the fracture. A different, medium-luminescence dolomite cement precipitated during (synkinematic) and after (postkinematic) the two main sets of fractures developed. Calcite cement is also present, but precipitation occurred only after all fractures formed (postkinematic) (Fig. 25). Qualitative element mapping on the SEM reveals that the low-luminescence dolomite is Fe rich and Mg poor, relative to the other dolomites. The distribution of postkinematic calcite, and, hence, open fractures, was variable. We observed fracture porosity in some fractures in the A1 well, but most fractures in the Unit #3 well were occluded by calcite.

Although it is not possible to know whether the fractures in the sidewall cores are part of the same set, owing to lack of crosscutting relations in the sidewall cores, they have the same temporal

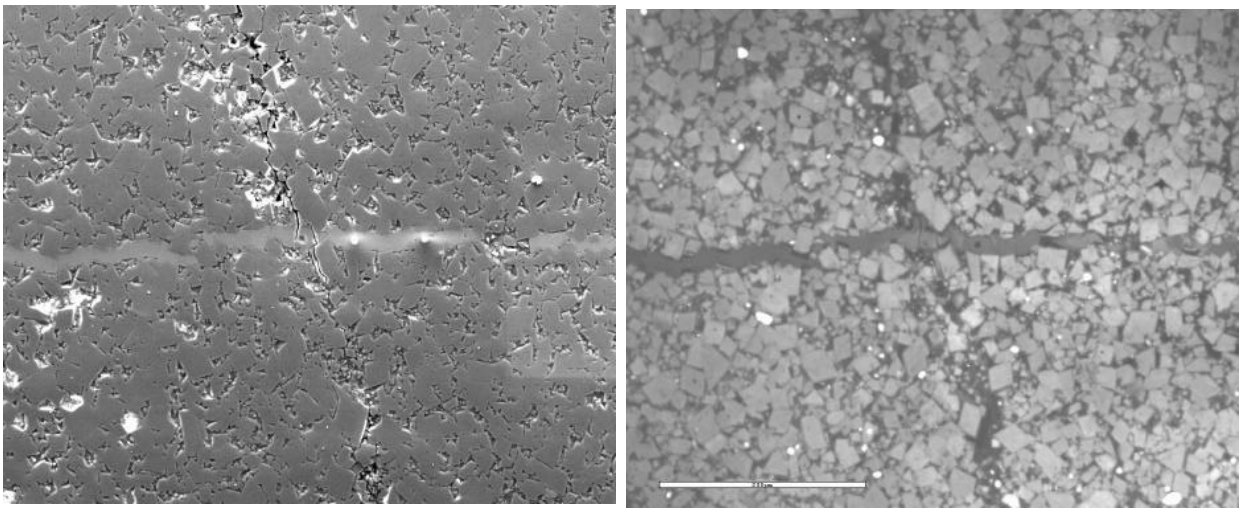

Figure 25. Secondary electron image (SEI) and cathodoluminescence image (CL) of fractures in theA1 well at 9055 ft. The fracture trending across the page from left to right is completely sealed. It contains very small amounts of low-luminescence dolomite (black) as a lining on the fracture wall (synkinematic cement) and is filled with a medium-luminescence postkinematic cement, which in the SEI image shows as pale-gray calcite, being distinct from the darker gray dolomite. Scale bar is 200 micrometers.

relationship with dolomite and calcite cements. Because the whole core could not be oriented, we cannot know which of the two fracture sets identified on the image log we have measured in the Unit #3 well. At this stage we consider it likely that the NE-trending fractures in the A1 well are contemporaneous with the dominant set at 9070 to 9079 ft in the Unit #3 well. Fracture orientations measured in the core were separated into different depth categories on the basis of dominant orientation of fractures in the image log over given depth ranges.

IV-4.1.2.4 Conclusions

Fractures that crosscut clasts and cement and therefore postdate brecciation were identified in the Unit #3 core. These fractures form continuous features in the core and have been identified on image logs in this well. Results from sidewall cores and borehole images from a recent well confirmed the orientation of two sets of fractures (S70E/90 and S30W/90) in Barnhart field. These fracture

sets appear to be broadly synchronous, but their origin has not yet been determined. They may be related to late-stage cave collapse or to some more regionally widespread tectonic event.

It is possible to measure fracture intensity of microfracture populations that are subsets of the fracture sets observed in the core using SEM-based cathodoluminescence techniques specially adapted for carbonate imaging. Fracture intensity was obtained for samples from different depths from two wells in Barnhart field. Intensity within wells was consistent, but the Unit #3 well showed a higher intensity than the A1 well. Samples from additional depths and other wells are required to confirm whether there are variable fracture intensities from well to well and to what extent each intensity level persists both vertically and laterally.

Postbrecciation fractures propagated along dolomite-grain boundaries, and therefore this fracturing event was interpreted to have occurred after dolomitization of the host rock. Two compositionally different dolomite cements precipitated during fracture opening and show crack-seal structure. The more abundant of these cements also precipitated after fracture opening, as did calcite. Calcite is responsible for occlusion of fracture porosity in the larger fractures. It is variably distributed. At this stage, although we cannot predict the distribution of calcite cements in Barnhart field, we can identify its presence on a site- specific basis using thin sections and thereby predict where large fractures would be sealed, even if we have not sampled them directly.

IV-4.2. Subtask 3.2 – Refining of Predictive Fracture Model

We are in the process of refining our interpretations of the fractures using new and existing core and log data to develop a predictive model for fracture types throughout the field. It will be an ongoing task through the end of the year.

IV-5. Task 4.0 – Characterization and Modeling of Rock Mechanical Properties and Fractures

The tasks in this section are still being considered. They may not have a bearing on the present study. Decisions on these tasks will be delayed until more data are obtained and analyzed.

IV-6. Task 5.0 – Experimental Characterization of Thermal Alteration

Exposure of rock to elevated temperatures can lead to the creation of abundant microfractures (Johnson and Gangi, 1980), which can, in turn, substantially alter mechanical and fluid transport properties (Bauer and Johnson, 1978).

IV-6.1. Subtask 5.1 – Measurement of Response to Simulated HPAI Conditions

We will carry out measurements of mechanical behavior of core material subjected to simulated HPAI conditions. Specimens prepared from core will be heated to appropriate temperatures and placed in a triaxial test chamber for the complete sequence of mechanical and fluid transport measurements. Measurements will be made on bulk deformation and failure behavior, permeability, pore volume, pore compressibility, and wave velocities.

IV-6.1.1. Measuring the Effect of Heating on Fractured Reservoir Rock

Laboratory testing is being carried out to quantitatively assess mechanical alterations of reservoir material by the elevated temperatures near the combustion front. The primary focus of initial studies is thermally generated microfractures. Published studies (Bauer and Johnson, 1978; Friedman and Johnson, 1978; Johnson and others, 1978; Johnson and others, 1987) have shown significant thermal microfracturing in rock from heating to temperatures of a few hundred degrees centigrade and that the microfracture fabric can result in significant alteration of mechanical and pore fluid transport behavior. Thermal-induced microfractures associated with in situ combustion temperatures in the range of 600° (Moore and others, 1997) may therefore affect combustion and recovery efficiency. In order to assess these effects, samples of core material were heated in steps of 100°C up to nominal in situ combustion temperatures of 600°C. Compressional wave velocity in rock is sensitive to crack density, and wave velocities in the test specimens were measured at room temperature following each temperature excursion.

Two samples of carbonate outcrop were used for testing-protocol development. Variations in wave velocity with temperature are shown in Figure 26. The substantial decreases in velocity are

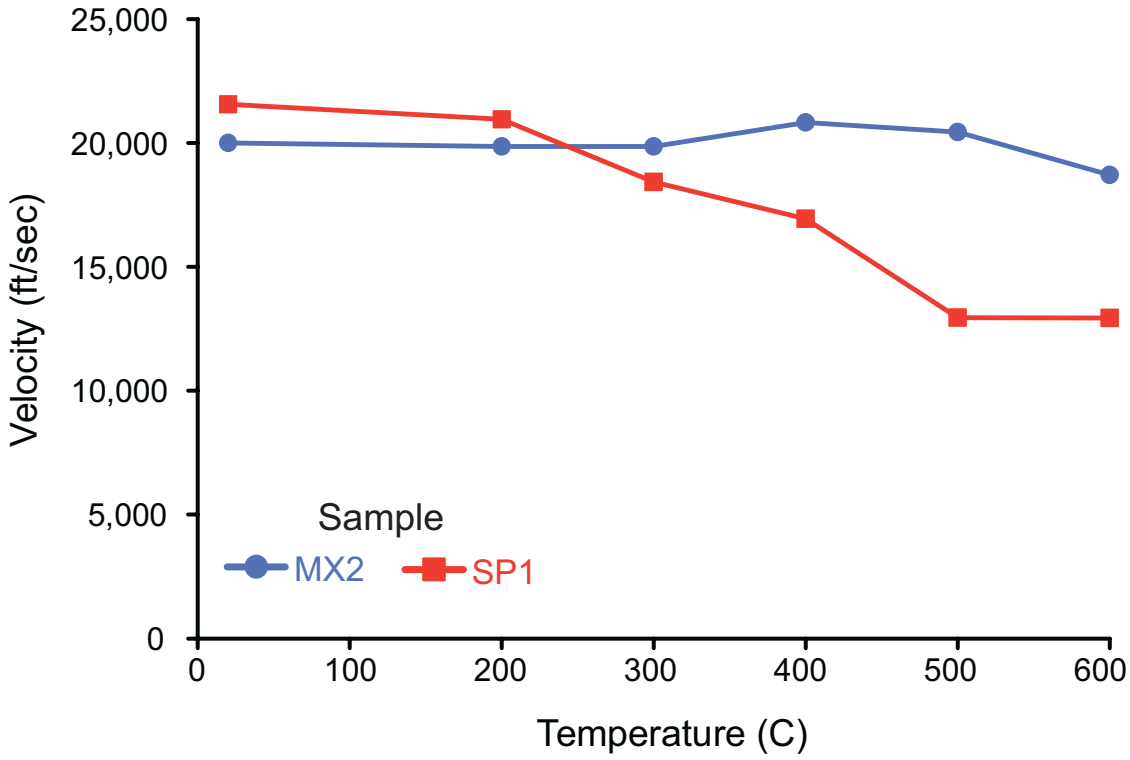

Figure 26. Measured variations in wave velocity at room temperature, following 15-minute heat sequences at the indicated temperatures.

consistent with changes found in granites. One specimen (SP1) contained numerous natural fractures, and this specimen showed a pronounced velocity decrease associated with thermally generated microfractures. The second sample, MX2, was relatively free of natural fractures and showed no crack-related velocity decrease. These observations suggest that thermal alteration would be strongly influenced by the existence of prior fracture events. This conclusion is based on preliminary experimentation but has some basis in theory: thermally generated microfractures are primarily related to local heterogeneities in thermal expansion (Johnson and others, 1978), and infill of naturally fractured rock should result in a greater degree of heterogeneity.

The two prototype heating tests were carried out on material in a completely unconfined state. It is known that fracturing is suppressed by confining stress (Friedman and others [1979]; however, the effects of confining pressure may be small at elevated temperature), and a core holder has been fabricated to provide for heating under confined conditions. The apparatus, shown schematically in

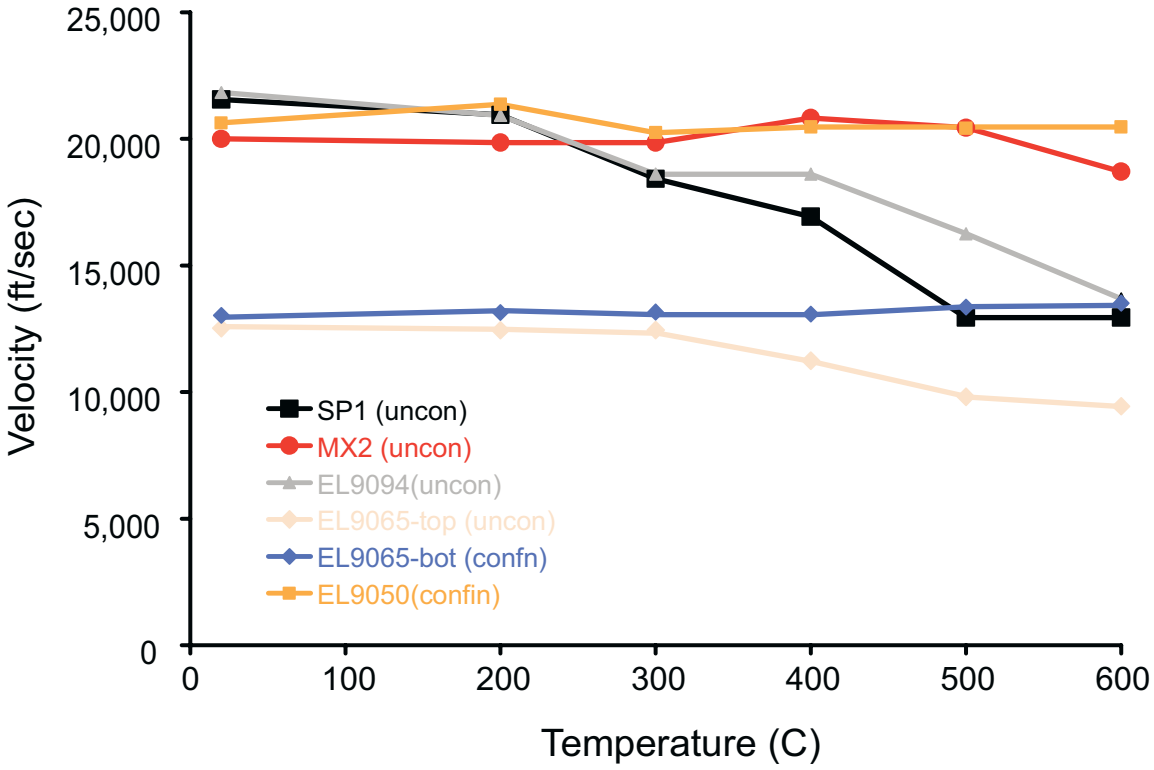

Figure 27. Schematic diagram of core holder for thermal cycle tests.

Figure 27, consists of an aluminum jacket, constructed to closely fit the outer surfaces of a 1-inch diameter by nominal 2-inch-long cylindrical specimen. Prior to testing, the sample is placed in the chamber and loaded to approximately 500 psi. While under stress, the walls of the core holder are tightened, and the top cap was secured by tightening the four set screws.

Measurements of the effects of thermal cycling on mechanical behavior are now being carried out for core samples from the Ellenberger Formation. Samples from the Unit #3 core from a variety of facies, both brecciated and intact, were selected for testing, and the slab face and up-hole cut surface were photographed prior to plugging. Preliminary macrofracture descriptions of these samples were made. Plugs measuring 2.65 cm (1 inch), with the long axis vertical, have been taken from five depths for velocity measurements during heating with and without a confining stress. Prior to testing, each of the sample ends was trimmed normal to the core axis. The trimmed end will be made into a thin section. Posttest thin sections will also be prepared to compare textures and microfracture patterns with the pretest sample.

The first test sequence was carried out on two plugs from a depth of 9,065 ft. This sample section is from the intact slab facies and has no observed natural macrofractures. One of the plugs (from the top of the core section) was heated unconfined, and the plug from the bottom of the section was heated while confined in the core holder. Plugs were then taken from core at depths of 9,050.1 and 9,094.3 ft. These plugs are from brecciated facies and potentially provide a contrast to the intact slab previously tested. We are interested in finding out whether naturally fractured samples behave differently from unfractured samples when heated. Sample 9050 was tested under confined conditions, and sample 9094 was tested under unconfined conditions.

The measured velocity variations for these specimens are shown in Figure 28. Results from the initial two tests are also included for comparison. None of the specimens tested under confined conditions showed any evidence of thermally induced microfracturing (i.e., no reduction in wave velocity), although all of the Ellenburger specimens—including the specimen from 9,065 ft that was visibly free of natural fractures—indicated significant thermal damage.

Two additional plugs were taken from core at depths 9,105 and 9,131 ft. The core from 9,105 ft is highly brecciated, and although a long section was drilled, only one intact plug, approximately 4 cm long, was obtained intact. However, this will be sufficient to run one test. The sample from 9,131 ft is not brecciated but has small fractures in two orientations distributed on a spacing of a few centimeters throughout the sample. These tests are currently under way.

A precise estimate of the confining stresses produced by the core holder requires values of thermal expansion coefficients and compressibilities of the test specimen and aluminum core holder. Mechanical and thermal properties of aluminum can be obtained from handbook tabulations, but the material-dependent values of the rock specimens must be determined experimentally. These values are also needed for the numerical simulations of fire-flood performance, and preparations for measurements of these parameters are under way.

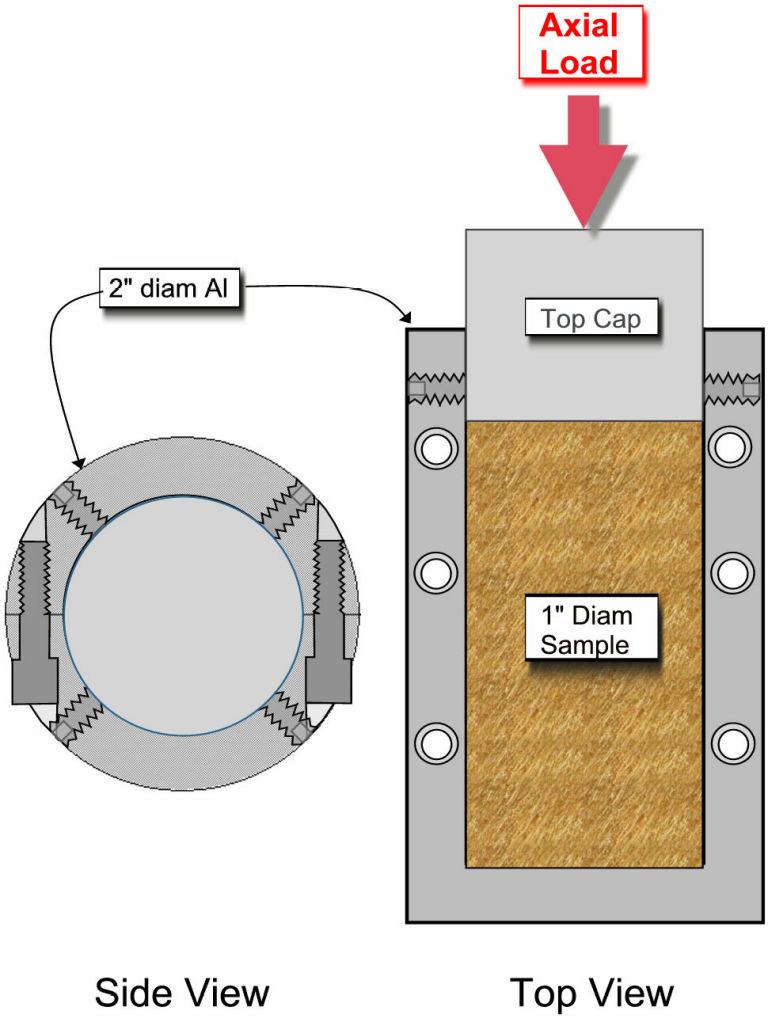

Figure 28. Summary of variations in wave velocity from elevated temperature cycles in carbonates.

IV-6.1.2. Modeling Reservoir Behavior

We have identified a reservoir simulation code (STARS) that includes the capability to model in situ combustion. In a review meeting with the operator, Goldrus Producing Company, we established that they have a large compiled database on production and completion for all the wells in the area of interest, which was compiled data from information held by University Lands. We will use these data to build a simulation.

Initially we will model a small volume that includes Goldrus's currently active injector and producer wells and their projected new wells. Information on wells outside this volume will also be used to characterize the reservoir behavior. Geological parameters, such as porosity distribution and fracture architecture established through studies of A-1 and A-6 sidewall cores and Unit #3 whole core, will be utilized in the model.

In order to run the STARS combustion simulation, we need to measure mechanics parameters from reservoir-specific rock from Barnhart field. We will use plugs to measure mechanical properties of bulk and pore compressibility and thermal expansion coefficients. We will use published values for calcite and dolomite for specific heat and published values for carbonates for thermal conductivity (published values for limestone and other carbonate rocks show little variation) and carry out sensitivity analyses to assess the degree of precision needed for these parameters.

V. PHASE 2: FIELD DEMONSTRATION

This phase will start during the second half of 2003, as noted on the Project Task Schedule, and will be discussed in the next semiannual review report.

VI. PHASE 3: TECHNOLOGY TRANSFER

The major phase of technology transfer will start at the beginning of 2004, as noted on the Project Task Schedule; however, several important technology transfer activities relative to this project have already been conducted. Of special significance among these activities was the presentation of oral, poster, and core poster presentations outlining the progress of the Barnhart reservoir study at a special workshop. This workshop, entitled "New Methods for Locating and Recovering Remaining Hydrocarbons in the Permian Basin, A Symposium and Workshop" was co- sponsored by the Bureau of Economic Geology, the Petroleum Technology Transfer Council, and the University Lands West Texas Operations. The symposium was presented to about 80 Permian Basin geologists, engineers, and managers in Midland/Odessa, Texas, in May. A poster presentation was also delivered at the annual convention of the AAPG in May. The titles of these presentations are:

1. Loucks, Bob, and Combs, Deanna, 2003, Pore networks in Lower Ordovician Ellenburger Group collapsed paleocave systems: examples from Barnhart field, Reagan County, Texas, presented at New Methods for Locating and Recovering Remaining Hydrocarbons in the Permian Basin, A Symposium and Workshop sponsored by the Bureau of Economic Geology, Petroleum Technology Transfer Council, and University Lands West Texas Operations. Symposium held at the Center for Energy and Economic Diversification, Midland/Odessa, Texas, May 29, 2003. (PowerPoint presentation)

2. Combs, D. M., Loucks, R. G., and Ruppel, S. C., 2003, Ellenburger Group collapsed paleocave facies, Barnhart field, Reagan County, Texas, presented at New Methods for Locating and Recovering Remaining Hydrocarbons in the Permian Basin, A Symposium and Workshop sponsored by the Bureau of Economic Geology, Petroleum Technology Transfer Council, and University Lands West Texas Operations. Symposium held at the Center for Energy and Economic Diversification, Midland/Odessa, Texas, May 29, 2003. (Poster presentation in pdf file format)

3. Gale, J. F. W., Gomez, L., Laubach, S. E., Marrett, R., Olson, J. E., Holder, J., and Reed, R. M., 2003, Predicting and characterizing fractures in the Ellenburger: using the link between diagenesis and fracturing, presented at New Methods for Locating and Recovering Remaining Hydrocarbons in the Permian Basin, A Symposium and Workshop sponsored by the Bureau of Economic Geology, Petroleum Technology Transfer Council, and University Lands West Texas Operations. Symposium held at the Center for Energy and Economic Diversification, Midland/Odessa, Texas, May 29, 2003. (PowerPoint presentation)

4. Gomez, L. A., Gale, J. F. W., Reed, R. M., Loucks, R. G., Ruppel, S. C., and Laubach, S. E., New techniques in fracture imaging and quantification: application in the Ellenburger Group in West Texas, presented at American Association Petroleum Geologist Annual Meeting, Salt Lake City, May 11-14. (Poster presentation in pdf file format)

VII. RESULTS AND DISCUSSION

The project is finishing its initial data-collection stage and is assembling the data into products that can be used to define the architecture and, hence, plumbing of the field. The best possible estimate of the plumbing of the field is essential to our understanding injector/producer relationships in order to analyze sweep patterns.

A basic understanding of the pore network is emerging, but more work is necessary to populate the field with correct pore types. As we define the host rock versus collapsed paleocave breccias and fractures, we will be able to apply our pore network model more accurately. New core and log data that we will obtain from Goldrus Producing Company this summer will help with this task.

The experimental work on the effects of high temperature is proceeding as planned. The test apparatus is providing the desired results. More testing needs to be completed before we can summarize results.

Goldrus Producing Company will be drilling several new wells in July of 2003. At least one of these wells will be cored, which will provide critically needed data. The next semiannual report should have some solid conclusions about the ability of high-pressure air injection on reviving Barnhart field.

VIII. CONCLUSION

The architecture of the field is nearly completed. It is allowing us to understand the distribution of reservoir quality rock. As the well tests and monitoring program progress we will be able to select injector/producer patterns on the basis of the plumbing in the field.

The complex pore network in this partly karsted field presents a challenge on how to populate a field model with reservoir quality data. Our research effort on this task is providing data that has not been available for other karsted fields. Separating collapsed-paleocave-associated fractures and interclast pores from tectonic-associated pores in cores is difficult and little research has been completed on this topic before this study. It will be a major engineering task to integrate these findings into a flow model.

The experimental data are providing information on the effect of high-temperature processes on the rocks, especially fracturing of the rocks. This information is an important contribution because it allows us to better understand the sweep efficiency in this relatively low-quality reservoir.

IX. REFERENCES

Bauer, S. J. and Johnson, B., 1978, Effects of slow uniform heating on the physical properties of the Westerly and Charcoal Granites: Proceedings of the 20th U.S. Symposium on Rock Mechanics, p. 7-18.

Combs, D. M., Loucks, R. G., and Ruppel, S. C., 2003, Ellenburger Group collapsed paleocave facies, Barnhart field, Reagan County, Texas, *in* New Methods for Locating and Recovering Remaining Hydrocarbons in the Permian Basin, A Symposium and Workshop sponsored by the Bureau of Economic Geology, Petroleum Technology Transfer Council, and University Lands West Texas Operations, Center for Energy and Economic Diversification, Midland/ Odessa, Texas, May 29.

Friedman, M., Handin, J., Higgs, N. G., and Lantz J. R., 1979, Strength and ductility of four dry igneous rocks at low pressures and temperatures to partial melting: Proceedings of the 23rd U.S. Symposium on Rock Mechanics, p. 79-290.

Friedman, M., and Johnson, B., 1978, Thermal cracks in unconfined Sioux quartzite: Proceedings of the 19th U.S. Symposium on Rock Mechanics, p. 423-430.

Gomez, L. A., Gale, J. F. W., Ruppel, S. C., and Laubach, S. E., 2001, Fracture characterization using rotary-drilled sidewall coves: an example from the Ellenburger Formation: Proceedings of the West Texas Geological Society Fall Meeting, WTGS publication, v. 01-110, p. 81-89.

Holtz, M. H., and Kerans, Charles, 1992, Characterization and classification of West Texas Ellenburger reservoirs, *in* Candelaria, M. P., and Reed, C. L., eds., Paleokarst, karst related

diagenesis and reservoir development: examples from Ordovician – Devonian age strata of West Texas and the Midcontinent: Permian Basin SEPM Publication 92-33, p. 45-54.

Johnson, B., Friedman, M., and Hopkins, T. W., 1987, Strength and microfracturing of Westerly granite extended wet and dry at temperatures to 800° C and pressures to 200 MPa: Proceedings of the 28th U.S. Symposium on Rock Mechanics, p. 399-412.

Johnson, B., Gangi, A. F., and Handin, J., 1978, Thermal cracking of rocks subjected to slow, uniform temperature changes: Proceedings of the 19th U.S. Symposium on Rock Mechanics, p. 259-267.

Laubach, S. E., 2003, Practical approaches to identifying sealed and open fractures: American Association of Petroleum Geologists Bulletin, v. 87, p. 561-579.

Laubach, S. E., Marrett, R. A., and Olson, J. E., 2000, New directions in fracture characterization: The Leading Edge, p. 704-711.

Loucks, R. G., 1999, Paleocave carbonate reservoirs: origins, burial-depth modifications, spatial complexity, and reservoir implications: American Association of Petroleum Geologists Bulletin, v. 83, p. 1795-1834.

Loucks, R. G., and Mescher, P., 2001, Paleocave facies classification and associated pore types: American Association of Petroleum Geologists, Southwest Section, Annual Meeting, Dallas, Texas, March 11–13, CD-ROM, 18 p.

Marrett, R., 1996, Aggregate properties of fracture populations: Journal of Structural Geology, v. 18, p. 169-178.

Marrett, R., Ortega, O., and Kelsey, C., 1999, Extent of power-law scaling for natural fractures in rock: Geology, v. 27, p. 799-802.

Moore, R. G., Laureshen, C. J., Belgrave, J. D. M., Ursenbach, M. G., and Mehta, S. A., 1997, In situ combustion in heavy oil reservoirs: problems and perspectives: In Situ, v. 21, p. 1-26.

Ortega, O., 2002, Fracture-size scaling and stratigraphic controls on fracture intensity: The University of Texas at Austin, Ph.D. dissertation.

Reed, R. M., and Milliken, K. L., 2003, How to overcome imaging problems associated with carbonate minerals on SEM-based cathodoluminescence systems: Journal of Sedimentary Research, v. 73, p. 326-330.